

There and Back Again: On the relation between Noise and Image Inversions in Diffusion Models

Lukasz Staniszewski^{1,2*}, Lukasz Kuciński^{3,4,5}, Kamil Deja^{1,2}

¹Warsaw University of Technology, ²IDEAS Research Institute, ³University of Warsaw

⁴Institute of Mathematics, Polish Academy of Sciences, ⁵IDEAS NCBR

Abstract

Diffusion Models achieve state-of-the-art performance in generating new samples but lack a low-dimensional latent space that encodes the data into meaningful features. Inversion-based methods address this by reversing the denoising trajectory, mapping each image back to its approximated starting noise. In this work, we thoroughly analyze this procedure and focus on the relation between the initial Gaussian noise, the generated samples, and their corresponding latent encodings obtained through the DDIM inversion. First, we show that latents exhibit structural patterns in the form of less diverse noise predicted for smooth image regions. As a consequence of this divergence, we present that the space of image inversions is notably less manipulative than the original Gaussian noise. Next, we explain the origin of the phenomenon, demonstrating that, during the first inversion steps, the noise prediction error is much more significant for the plain areas than for the rest of the image. As a surprisingly simple solution, we propose to replace the first DDIM Inversion steps with a forward diffusion process, which successfully decorrelates latent encodings, leading to higher quality editions and interpolations. The code is available at <https://github.com/luk-st/ta>.

1 Introduction

Diffusion-based probabilistic models (DMs) [49], have achieved state-of-the-art results in many generative domains including image [8], speech [43], video [17], and music [34] synthesis. Nevertheless, one of the significant drawbacks that distinguishes diffusion-based approaches from other generative models like Variational Autoencoders (VAEs) [26] is the lack of an implicit latent space that encodes the images into low-dimensional, interpretable, or editable representations. To mitigate this issue, several works seek meaningful relations in the starting noise used for generations. This method, known as an inversion technique, was introduced with Denoising Diffusion Implicit Models (DDIM) [50], but led to the proliferation of works [12, 38, 19, 35, 18, 41]. The core idea is to use a denoising diffusion model to predict noise and add it to the image instead of subtracting it. Repeating this process effectively traces the backward diffusion trajectory, approximating the original *noise* that could have generated the *image*. However, due to approximation errors and biases introduced by the trained denoising model, discrepancies arise between the initial Gaussian noise and the reconstructed *latent* representation.

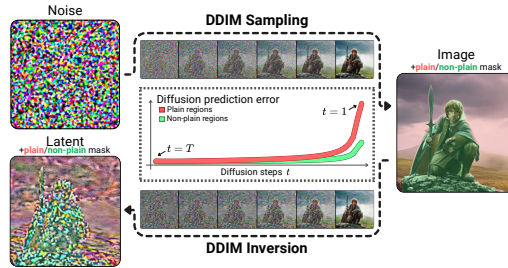


Figure 1: **DDIM inversion produces latent encodings that exhibit less diverse noise in the smooth image areas than in the non-plain one.** We attribute this problem to the errors of noise prediction in the first inversion steps.

introduced with Denoising Diffusion Implicit Models (DDIM) [50], but led to the proliferation of works [12, 38, 19, 35, 18, 41]. The core idea is to use a denoising diffusion model to predict noise and add it to the image instead of subtracting it. Repeating this process effectively traces the backward diffusion trajectory, approximating the original *noise* that could have generated the *image*. However, due to approximation errors and biases introduced by the trained denoising model, discrepancies arise between the initial Gaussian noise and the reconstructed *latent* representation.

*Corresponding author: luks.staniszewski@gmail.com

While recent works [12, 38, 41, 19, 63] try to improve the inversion procedure from the perspective of tasks such as image reconstruction, editing, or interpolation, in this work, we focus on the inversion process itself and analyze the errors DDIM inversion introduces. To that end, we analyze the relation between sampled Gaussian noise, generated images, and their inverted latent encodings. First, we review existing studies and conduct additional analyses demonstrating that the reverse DDIM technique produces latent representations with pixel correlations that deviate significantly from a Normal distribution. As presented in fig. 1, we experimentally show that this deviation manifests as lower diversity in latent codes, particularly in regions corresponding to smooth image surfaces. We further attribute this discrepancy to the observation that the approximation error of DDIM inversion is higher for pixels representing smooth areas than for other parts of the image. Additionally, we show that this error discrepancy occurs predominantly during the initial steps of the inversion process. To present the consequences of the observed divergence, we analyze the effects of using latent variables instead of raw noise in practical DM applications. Our results show that the latent space is less adaptable for manipulation than the noise space. This limitation is particularly noticeable in lower-quality interpolations between randomly chosen latents and less expressive edits, especially in smooth regions of source images.

Finally, to mitigate the issue, we propose a surprisingly simple solution, which is replacing the first steps of the DDIM inversion process with a forward diffusion. In the final experiments, we show that such an approach successfully decorrelates the resulting latents, mitigating observed limitations, without degrading the reconstruction quality. Our main contributions can be summarized as follows:

- We show that reverse DDIM produces latent representations that deviate from the Normal distribution mostly because of less diverse values for the parts of the latents corresponding to the plain image surfaces.
- We explain the origin of this phenomenon, showing that the inversion approximation error is more notable for the plain pixel areas, especially during the first noising steps.
- We show that as a consequence of this divergence, the resulting latent space is less manipulative, which leads to the lower quality of interpolations and edits generated from latent variables as a starting state.
- We propose a simple yet effective solution to the problem by substituting early DDIM inversion steps with forward diffusion.

2 Background and Related Work

Denoising Diffusion Implicit Models. The training of DMs consists of forward and backward diffusion processes, where in the context of Denoising Diffusion Probabilistic Models (DDPMs [16]), the former one with training image x_0 and a variance schedule $\{\beta_t\}_{t=1}^T$, can be expressed as $x_t = \sqrt{\alpha_t}x_0 + \sqrt{1 - \alpha_t}\epsilon_t$, with $\alpha_t = 1 - \beta_t$, $\bar{\alpha}_t = \prod_{s=1}^t \alpha_s$, and $\epsilon_t \sim \mathcal{N}(0, \mathcal{I})$.

In the backward process, the noise is gradually removed starting from a random noise $x_T \sim \mathcal{N}(0, \mathcal{I})$ for $t = T \dots 1$, with intermediate steps defined as:

$$x_{t-1} = \sqrt{\bar{\alpha}_{t-1}} \cdot \underbrace{(x_t - \sqrt{1 - \bar{\alpha}_t} \cdot \epsilon_\theta^{(t)}(x_t, c)) / \sqrt{\bar{\alpha}_t}}_{x_0 \text{ prediction}} + \underbrace{\sqrt{1 - \bar{\alpha}_{t-1} - \sigma_t^2} \cdot \epsilon_\theta^{(t)}(x_t, c)}_{\text{direction pointing to } x_t} + \sigma_t z_t, \quad (1)$$

where $\epsilon_\theta^{(t)}(x_t, c)$ is an output of a neural network (such as U-Net), and can be expressed as a combination of clean image (x_0) prediction, a direction pointing to previous denoising step (x_t), and a stochastic factor $\sigma_t z_t$, where $\sigma_t = \eta \sqrt{\beta_t(1 - \bar{\alpha}_{t-1}) / (1 - \bar{\alpha}_t)}$ and $z_t \sim \mathcal{N}(0, \mathcal{I})$. In the standard DDPM model [16], the η parameter is set to $\eta = 1$. However, changing it to $\eta = 0$ makes the whole process a deterministic Denoising Diffusion Implicit Model (DDIM) [50], a class of DMs we target in this work.

One of the advantages of DDIM is that by making the process deterministic, we can encode images back to the noise space. The inversion can be obtained by rewriting eq. (1) as

$$x_t = \sqrt{\alpha_t}x_{t-1} + (\sqrt{1 - \bar{\alpha}_t} - \sqrt{\alpha_t - \bar{\alpha}_t}) \cdot \epsilon_\theta^{(t)}(x_t, c) \quad (2)$$

However, due to circular dependency on $\epsilon_\theta^{(t)}(x_t, c)$, Dhariwal and Nichol [8] propose to approximate this equation by assuming the local linearity between directions ($x_{t-1} \rightarrow x_t$) and ($x_t \rightarrow x_{t+1}$), so

that the model’s prediction in t -th inversion step can be approximated using x_{t-1} as an input, i.e.,

$$\epsilon_{\theta}^{(t)}(x_t, c) \approx \epsilon_{\theta}^{(t)}(x_{t-1}, c). \quad (3)$$

While such approximation is often sufficient to obtain good reconstructions of images, it introduces the error dependent on the difference $(x_t - x_{t-1})$, which can be detrimental for models that sample images with a few diffusion steps or use the classifier-free guidance [15, 38] for better prompt adherence. As a result, also noticed by recent works [12, 41], latents resulting from DDIM inversion do not follow the definition of Gaussian noise because of the existing correlations. In this work, we empirically study this phenomenon and explain its origin. We discuss the relations between the following three variables: **Gaussian noise** (x_T , an input to generate an image through a backward diffusion process), **image sample** (x_0 , the outcome of the diffusion model generation process), and **latent encoding** (\hat{x}_T , the result of the DDIM inversion procedure as introduced in eq. (2)).

Image-to-noise inversion techniques. The DDIM inversion, despite the noise approximation errors, forms the foundation for many applications, including inpainting [58], interpolation [8, 63], and edition [53, 23, 14, 3, 7]. Several works [38, 12, 19, 35, 18, 37, 13, 4, 9, 62, 41, 54, 55, 40, 56, 2, 32, 20] aim to reverse the denoising process in text-to-image models, where prompt embeddings can strongly affect the final latent representation through Classifier-free-guidance (CFG) [15]. Null-text inversion [38] extends the DDIM inversion with additional null-embedding optimization, reducing the image reconstruction error. Other techniques improve inversion for image editing through seeking embeddings [37, 13, 9] or leveraging DDIM latents [4] for guidance. On the other hand, some works leverage additional numerical methods [35, 40, 12] to minimize inversion error. In particular, Renoise [12] iteratively improves the estimation of the next point along the forward diffusion trajectory by averaging multiple noise predictions with an additional patch-level regularization term penalizing pixel pairs’ correlations to ensure the latents’ editability. Huberman-Spiegelglas et al. [19] followed by Brack et al. [2] propose inversion methods for DDPMs, enabling the creation of various image edition results via inversion. Finally, to reduce the discrepancy between DDIM latents and Gaussian noises, Parmar et al. [41] propose to additionally regularize final DDIM Inversion outputs for better image editing, Lin et al. [32] introduce an alternative noise scheduler to improve inversion stability, while Hong et al. [18] propose an exact inversion procedure for higher-order DPM-Solvers, solving the optimization problem at each step.

3 Experiments

For thorough evaluation, we employ six different diffusion models working directly in the pixel space or latent space of the autoencoder described in table 1. For conditioning, we take prompts from the Recap-COCO-30K dataset [31] for IF and ImageNet class names for DiT. However, as noted

	ADM-32	ADM-64	ADM-256	LDM	DiT	IF
Diffusion	Pixel	Pixel	Pixel	Latent	Latent	Pixel
Image res.	32 × 32	64 × 64	256 × 256	256 × 256	256 × 256	64 × 64
Latent res.	-	-	-	3 × 64 × 64	4 × 32 × 32	-
Trainset	CIFAR-10	ImageNet	ImageNet	CelebA	ImageNet	LAION-A
Cond?	✗	✗	✗	✗	✓	✓
Backbone	U-Net	U-Net	U-Net	U-Net	DiT	U-Net

Table 1: **Overview of diffusion models used for our experiments.** We study both unconditioned and conditioned models, operating in pixel and latent spaces.

by Mokady et al. [38], cfg introduces additional errors to the DDIM inversion, so to focus solely on the inversion approximation error in our setup, we disable cfg by setting the guidance scale to $w = 1$. For both generation and inversion processes, we use the DDIM sampler with, unless stated otherwise, $T = 100$ sampling steps. This choice² aligns with prior works [18, 12, 24] using from 50 up to 200 inversion steps as a proper balance between reconstruction quality and short algorithm runtime.

3.1 Latents vs. noise

Prior work and findings. The reversed sampling (inversion) process provides the foundation for practical methods in many applications. The underlying assumption of those methods is that by encoding the *image* back with a denoising model, we can obtain the original *noise* that can be used for reconstruction. However, this assumption is not always fulfilled, which leads to the first question:

²We provide more discussion on the impact of sampling steps on observed inversion errors in appendix E.

Research Question 1: Are there any differences between sampled Gaussian noise and latents calculated through the DDIM inversion?

This question relates to several observations from the existing literature, which highlight that outputs of the DDIM inversion differ from the standard Gaussian noise [41, 12] and that the difference can be attributed to the approximation error [18, 55, 32]. In particular, Parmar et al. [41], followed by Garibi et al. [12], observe that latents “do not follow the statistical properties of uncorrelated, Gaussian white noise, causing poor editability”.

Experiments. First, we consolidate existing claims on the presence of correlations in the latent encodings (\hat{x}_T) by running an initial experiment that compares latents to images (x_0) and noises (x_T) across diverse diffusion architectures. In table 2, we calculate a mean of top-20 Pearson correlation coefficients (their absolute values) inside $C \times 8 \times 8$ pixel patches, where C is the number of channels (pixel RGB colors or latent space dimensions for latent models). The results, calculated with 10000 samples, confirm that latent representations have significantly more correlated pixels than the independent Gaussian noises. In fig. 2, we show how the measured correlations manifest themselves in the latent codes calculated with inverse DDIM. For pixel models such as Deepfloyd IF, we observe clear groups of correlated pixels as presented in fig. 1a. For latent diffusion models, we can highlight the inversion error by plotting the difference between the latent and the noise, as presented in fig. 1b. This property also holds for LDMs with a 4-channel latent space, where we use PCA to show the differences between the latents and noise for the DiT model (fig. 1c).

Conclusion. Recent studies, supported by our initial experiments, demonstrate that latent representations computed using the DDIM inversion deviate from the expected characteristics of independent Gaussian noise. Specifically, both visual analysis and quantitative evaluations reveal significant correlations between the neighboring pixels.

3.2 Location of latent encodings space

In this work, we propose to delve further and empirically analyze the nature of this issue. To that end, we first pose the following question:

Research Question 2: Is there a common characteristic of the latent encodings that distinguishes them from Gaussian noise?

Experiments. To answer this question, we first investigate the geometric aspect of how the latent encodings are distributed in relation to the original noise and generated samples. In table 3, we determine the most probable angles formed by noises x_T , samples x_0 , and latents \hat{x}_T for each model by binning the empirically observed angles and selecting those that satisfy the triangle angle sum, while maximizing the joint probability. We provide details on this methodology and visualizations in appendix F. Results of the experiment show that the angle located at the image and noise vertices (accordingly $\angle x_0$ and $\angle x_T$) are always acute and, in almost every case, the angle by the latent vertex ($\angle \hat{x}_T$) is obtuse. This property implies that, due to approximation errors in the reverse DDIM process,

Model	Noise (x_T)	Latent (\hat{x}_T)	Sample (x_0)
ADM-32	0.039 \pm .003	0.382 \pm .010	0.964 \pm .022
ADM-64	0.039 \pm .003	0.126 \pm .008	0.925 \pm .021
ADM-256	0.039 \pm .003	0.161 \pm .013	0.960 \pm .008
IF	0.039 \pm .003	0.498 \pm .025	0.936 \pm .019
LDM	0.039 \pm .003	0.045 \pm .014	0.645 \pm .099
DiT	0.041 \pm .003	0.103 \pm .021	0.748 \pm .064

Table 2: **Mean of top-20 Pearson correlation coefficients inside 8×8 patches for random Gaussian noises, latent encodings, and generations.** Latents created with the reverse DDIM are much more correlated than noises.

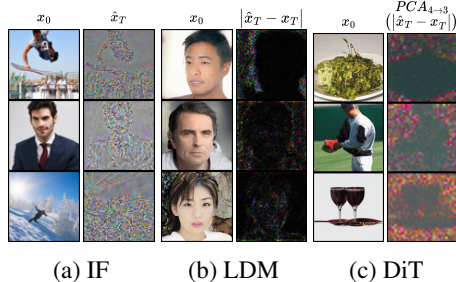


Figure 2: **Latent encodings exhibit image patterns.** For small pixel-space models (a), we observe correlations directly in the inversion results. For larger models (e.g., LDMs), the same patterns can be observed in the absolute errors between the latent and noise (b). This observation also holds for LDM models operating on 4-channels, where we use PCA for visualization (c).

Model	$\angle \mathbf{x}_0$	$\angle \mathbf{x}_T$	$\angle \hat{\mathbf{x}}_T$
ADM-32	29	28	123
ADM-64	11	60	109
ADM-256	24	73	83
IF	34	40	106
LDM	2	76	102
DiT	4	66	110

Table 3: **Most probable angles next to the Gaussian noise \mathbf{x}_T , generations \mathbf{x}_0 , and latents $\hat{\mathbf{x}}_T$ across different diffusion models.**

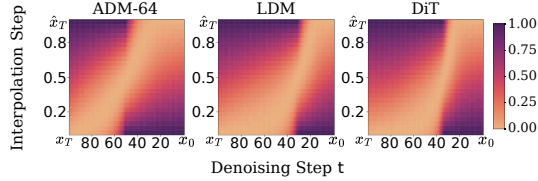


Figure 3: l_2 -distances between intermediate diffusion denoising steps x_t and points on the linear interpolation path from noise \mathbf{x}_T to the inverted latents $\hat{\mathbf{x}}_T$. The consecutive intermediate generation steps along the sampling trajectory consequently approach the latent.

ADM-32	ADM-64	ADM-256	IF	LDM	DiT	Noise
0.18 ± 0.33	0.71 ± 1.05	0.82 ± 1.27	0.29 ± 0.53	0.98 ± 1.40	0.89 ± 1.29	1.00

Table 4: **Variance of the latent encodings ($\hat{\mathbf{x}}_T$) calculated with different models.** In comparison, by definition, the variance of initial Gaussian noise equals 1.0.

latents reside in proximity to, but with a measurable offset, from the shortest-path trajectory between the noise distribution and the generated image.

However, the trajectory defined by the backward diffusion process does not necessarily follow the linear path, as DMs learn a highly non-linear score function, causing the denoising path to follow the curved structure of the data manifold [51]. Therefore, to strengthen our analysis further, we investigate the location of the latent with respect to the generation trajectory. To that end, we analyze the distance between the following steps $\{x_t\}_{t=T \dots 1}$ of the backward diffusion process and intermediate points on the linear interpolation path between the noise and the associated latent. We present the results of this experiment in fig. 3, where each pixel, with coordinates (t, λ) , is colored according to the l_2 distance between the intermediate trajectory step x_t and the corresponding interpolation step. This distance can be expressed as $\|(1 - \lambda)\mathbf{x}_T + \lambda\hat{\mathbf{x}}_T - x_t\|_2$.

We observe that, while moving from the random Gaussian noise (\mathbf{x}_T) towards the final sample (\mathbf{x}_0), the intermediate steps x_t approach the latent ($\hat{\mathbf{x}}_T$), while after the transition point present around 50-70% of the generative trajectory the distance to the latent becomes lower than the distance to the starting noise. **This observation reveals that latent encodings retain some characteristics of the original input samples and contain information about the source generation.**

To more closely localize the latent encodings, we propose to study their relations to the center of the analyzed space, point 0 being the mean of the initial noise \mathbf{x}_T . In table 4, we show the average variance of the latent encodings for randomly sampled and inverted 10,000 images. Latent encodings $\hat{\mathbf{x}}_T$ have, in general, lower variance than the noise, which means that the inversion process drives them towards the mean of the Gaussian distribution. The remaining question is, how does it manifest?

The visualizations shown in fig. 2 indicate that, in some cases, we can distinguish the structure of the original objects in the latent encodings. In particular, while the pixels associated with the objects have high diversity, which is also expected for white Gaussian noise, the areas related to the background are much smoother. This finding leads to the hypothesis that the most significant difference between the initial Gaussian noises and latent encodings is the limited variance in the areas corresponding to the background of the generated images. To validate it, we compare the properties of the resulting latents between plain and non-plain areas in the image. We determine binary masks \mathcal{M}_p that select smooth surfaces in the image, according to the neighbor differences described in appendix G. In table 5, we show that the error between the starting noise \mathbf{x}_T and the latent $\hat{\mathbf{x}}_T$ resulting from the DDIM inversion is higher for pixels corresponding to the plain areas. Across all the models, this trend goes along with a decrease in the standard deviation of the latents' pixels related to those image regions. It suggests that DDIM inversion struggles with reversing the plain image areas, bringing them to 0 (average) and reducing their diversity.

Model	Mean Absolute Error		Standard Deviation	
	Plain	Non-plain	Plain	Non-plain
ADM-32	0.49	0.43	0.34	0.46
ADM-64	0.22	0.15	0.49	0.64
ADM-256	0.39	0.29	0.53	0.66
IF	0.56	0.40	0.46	0.72
LDM	0.13	0.03	0.45	0.59
DiT	0.12	0.06	0.43	0.54

Table 5: **Average per-pixel absolute error (between noise and latent) and standard deviation of the latents' pixels corresponding to the plain and non-plain areas of generations.** The error for plain pixels, where latents are less diverse, is higher than for other regions.

Conclusion. Latent encodings resulting from the DDIM Inversion deviate from the Gaussian noise towards zero values. This can be attributed to the less diverse values for parts of the latents corresponding to the plain image surfaces. This observation reveals that latent encodings retain some characteristics of the original input samples and contain information about the source generation.

3.3 Origin of the divergence

Given the observation from the previous section, we now investigate the source of the correlations occurring in latent encodings, posing the question:

Research Question 3: What causes the spatial correlations observed in DDIM latents?

Experiments. We first recall that the DDIM Inversion error can be attributed to the approximation of the diffusion model’s output at step $t \in 1 \dots T$ with the output from step $t - 1$ (see eq. (3)). Hence, we can define the inversion approximation error for step t as the difference between DM’s output for the target and previous timesteps t and $t - 1$ as:

$$\xi(t) = \underbrace{|\epsilon_{\theta}^{(t)}(x_t, c) - \epsilon_{\theta}^{(t)}(x_{t-1}, c)|}_{\mathcal{E}_t^I}, \quad (4)$$

where \mathcal{E}_t^S is the true model prediction at step t , and \mathcal{E}_t^I is the inversion’s approximation using the previous step’s output. Based on the observations from the previous section, we propose to investigate how the inversion approximation error $\xi(t)$ differs for pixels associated with plain and non-plain image areas throughout the inversion process. To that end, we average the approximation errors for 4000 images for each of the $T = 50$ diffusion timesteps. To ascertain that we measure the error solely for the analyzed step t , we start the inversion procedure from the exact latent from step $(t - 1)$ (obtained from the sampling path). We split the latent pixels into plain and non-plain areas according to the masks calculated for clean images. More details on the experimental setup can be found in appendix H.

In fig. 4, we present the visualization of calculated differences for each diffusion step. There is a significant difference in the prediction errors for plain and non-plain areas, especially in the initial steps of the noising process. Additionally, in table 6, we show the actual values of the approximation error. By splitting the inversion process into two parts, we can observe that the first 10% of inversion steps contribute more to the overall error than the remaining 90%. Notably, the error in plain areas predominantly accumulates within the first 10% of the inversion steps.

Those observations can be related to recent works [29, 32] that analyze why numerical solvers incur significant errors during the earliest diffusion steps (as $t \rightarrow 0$). Specifically, Lee et al. [29] trace the error to the $1/t$ curvature blow-up of the reverse-time ODE trajectory, whereas Lin et al. [32] attribute the predominance of early DDIM inversion approximations to a singularity arising from commonly used noise schedules. Our experiments extend those studies by showing that the approximation error can mainly be attributed to the plain regions in the original images.

Conclusion. Early approximations during the DDIM Inversion procedure lead to unequally distributed errors for pixels related to the plain and non-plain image areas, making it the origin of structural patterns and correlations exhibited by the latent encodings.

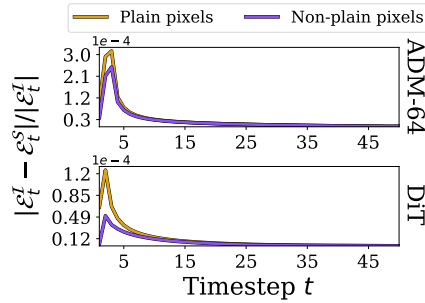


Figure 4: **Inversion approximation error is significantly higher during the first steps of the inversion process than for the next steps.** Moreover, in the first steps, errors for plain areas contribute more significantly to the error than errors for non-plain pixels.

Pixel area	Diffusion steps		Model	
			ADM-64	DiT
Plain	1, 2 ... 50	100%	15.11	5.67
Non-plain			12.43	3.16
Plain	1, 2 ... 5	10%	9.23	3.41
Non-plain			6.80	1.42
Plain	6, 7 ... 50	90%	5.87	2.23
Non-plain			5.63	1.74

Table 6: **Total per-pixel inversion error (normalized) over different timestep ranges $\mathcal{E}_{(t_s, t_e)}^E$ for plain and non-plain areas.** Inversion approximation error is higher for pixels related to plain image areas, especially in the first 10% of inversion steps.

Inversion steps replaced by forward (% T)	DiT			IF		
	Pixel Corr.	Reconstruction Absolute Error	KL Div. $\times 10^{-3}$	Pixel Corr.	Reconstruction Absolute Error	KL Div. $\times 10^{-3}$
Noise x_T	0.04	0.00	0.20	0.05	0.00	0.40
DDIM latent \hat{x}_T	0.16	0.05	11.57	0.64	0.07	608.25
1 (2%)	0.04	0.05	0.29	0.06	0.07	0.98
1...2 (4%)	0.04	0.07	0.25	0.05	0.07	0.48
1...5 (10%)	0.04	0.12	0.49	0.05	0.08	0.42
1...10 (20%)	0.04	0.15	0.45	0.05	0.10	0.40

Table 7: **Structures can be removed from DDIM latents by replacing inversion steps with forward diffusion.** Using forward diffusion instead of the first 4% of inversion steps brings the resulting latents closer to Gaussian noise without a major degradation in the image reconstruction.

Model	Region	Different prompt generations from:		
		Noise (baseline)	Latent DDIM Inv.	Latent w/ Forward 4%
IF	Plain	17.90	14.92 (+16.7%)	17.42 (+2.7%)
	Non-plain	18.60	17.35 (+6.7%)	18.16 (+2.4%)
DiT	Plain	13.64	11.95 (+12.4%)	13.27 (+2.7%)
	Non-plain	16.49	15.34 (+7.0%)	16.18 (+1.9%)

Table 8: **PNG bit-rate (bits / pixel) after saving only the masked pixels.** Higher compression (lower bpp) means less local variability in the pixel stream. Values in parentheses are the percentage change with respect to the noise baseline.

4 Consequences of the divergence and how to fix them?

After identifying the differences between the Gaussian noises and latents and highlighting the origin of this phenomenon, we finally pose the last question:

Research Question 4: What are the practical consequences of the divergence between noises and inverse DDIM latents, and how to fix them?

Building on top of our findings in section 3.3, which indicated that the initial inversion steps predominantly contribute to the divergence between latent variables and Gaussian noise, we propose to decorrelate the final DDIM latents by replacing the first inversion steps with random Gaussian noise $\epsilon \sim \mathcal{N}(0; \mathcal{I})$ as in the standard forward diffusion process (see appendix I for pseudocode):

$$x_t = \begin{cases} \sqrt{\bar{\alpha}_t}x_0 + \sqrt{1 - \bar{\alpha}_t}\epsilon, & \text{if } t \leq t' \quad (\text{Forward Diffusion}) \\ \sqrt{\bar{\alpha}_t}x_{t-1} + (\sqrt{1 - \bar{\alpha}_t} - \sqrt{\alpha_t - \bar{\alpha}_t}) \cdot \epsilon_\theta^{(t)}(x_{t-1}, c), & \text{if } t > t' \quad (\text{DDIM Inversion}) \end{cases} \quad (5)$$

We first evaluate the effectiveness of this technique, with $N = 10000$ images generated with $T = 50$ diffusion steps using DiT and IF models. For such generations, we first noise them with a forward diffusion to the intermediate step t' , followed by the DDIM inversion for $T - t'$ steps, starting from the $x_{t'}$ and ending up with a new approximation of the starting noise. In table 7, we show that by replacing just 4% of the inversion steps, we can completely remove correlations in the latents, up to the level of random Gaussian noise. Moreover, in table 8, we measure the size of the different parts of images (plain vs non-plain) after saving them with the PNG lossless compression. As is visible, compression is the most effective in the parts related to plain images generated from the DDIM latents, which inclines low diversity of their values. At the same time, replacing only 4% of inversion steps significantly reduces this issue. In the following sections, we showcase several consequences of the divergence between noises and latents and how our simple solution reduces those issues.

4.1 Interpolation quality

We start with the task of image interpolation, where the goal, for two given images, is to generate a sequence of semantically meaningful intermediary frames. Numerous methods [8, 50, 47, 63, 60, 1] leverage diffusion models to obtain realistic transitions. Song et al. [50] propose to use the latent variables resulting from the DDIM inversion technique and interpolate them with the spherical linear interpolation (SLERP [48]), that, for two objects x and y , with an interpolation coefficient $\lambda \in [0, 1]$, is defined as $z(\lambda) = \frac{\sin((1-\lambda)\theta)}{\sin \theta}x + \frac{\sin \lambda\theta}{\sin \theta}y$, where $\theta = \arccos((x \cdot y)/(\|x\|\|y\|))$.

We compare the quality of interpolations in the noise and latent spaces. To this end, we sample $N = 20k$ noises, use DDIM with $T = 50$ diffusion steps to generate images, and invert those images back into the latents. Next, we randomly assign pairs of either two noises or latents, which we interpolate with SLERP for $\lambda \in \{0, \frac{1}{6}, \frac{1}{3}, \frac{1}{2}, \frac{2}{3}, \frac{5}{6}, 1\}$ and denoise. In fig. 5, we show that, by calculating FID-10k, intermediate noise generations preserve consistent quality along the entire interpolation path – meaning that all interpolated images fall into the real images manifold. In contrast, this property collapses for the setting with latents as inputs. In the following rows, we show that worse interpolation results for latents stem from the decline in the variety of produced generations, as indicated by a lower recall [27], especially in the middle of the interpolation path. Nevertheless, as presented in table 9, replacing only the first step of the DDIM inversion with the forward diffusion significantly reduces the issue, leading almost to the quality of the interpolations between ground-truth noises.

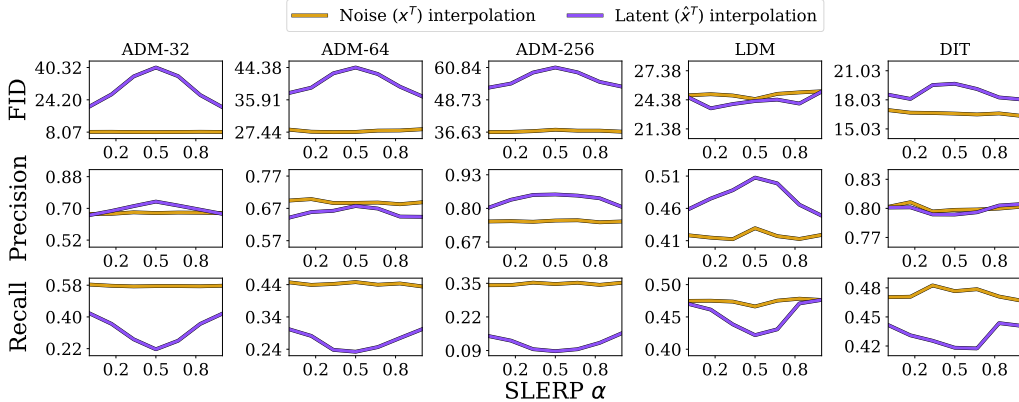


Figure 5: **The quality of images generated from spherical linear interpolations of latents \hat{x}_T deteriorates along the interpolation path, as indicated by the FID peak in the middle.** In contrast, the quality of generations from noise x_T interpolations remains stable. Recall metric reveals that the latent interpolation leads to the generation of much less diversity than noise.

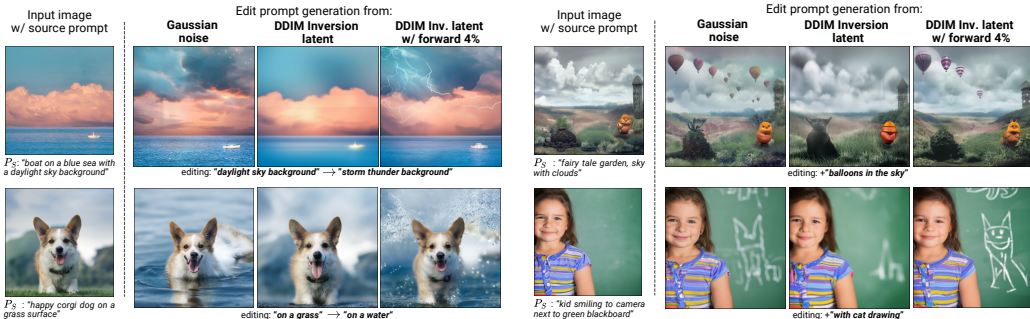


Figure 6: **Image edition by reversing the original image with a source prompt and reconstructing it with a target one.** DDIM Inversion produces less diverse image changes when the manipulation is related to plain regions in source images, contrary to when using ground-truth Gaussian noise. Replacing the first steps of DDIM Inversion with forward diffusion leads to more editable latents.

4.2 Diversity and quality of image edition

Text-to-image diffusion models with DDIM inversion are often used to modify images [14, 38, 12, 19]. However, knowing that DDIM latents are less diverse in plain areas, we hypothesize that using them as a starting point might reduce the diversity and quality of the edited samples. To evaluate this, we leverage DiT [42] and IF [52] as conditional DMs with $T = 50$ diffusion steps. For each model, we construct two sets of 1280 randomly selected prompts (ImageNet classes for DiT, COCO-30K [31] prompts for IF): (1) source prompts P_S , used during the generation and inversion, and (2) target prompts P_T , used for edition. Using source prompts P_S , we generate images I_S from Gaussian noise x_T and invert them back into the latents \hat{x}_T . Next, we regenerate images \hat{I}_T from the latents, changing the conditioning to the target prompts P_T . We compare the edits with ground truth targets I_T generated from the original noise x_T with P_T . In fig. 6, we present the drawback of leveraging latent variables as starting points for the denoising, where the I_S images' structures in the latents limit editing performance at those locations in \hat{I}_T images.

In table 10, we quantitatively measure this effect. First, we calculate the diversity of target generations (I_T, \hat{I}_T) against source images (I_S) . We use DreamSim distance [11], LPIPS [61], SSIM [57], and cosine similarity of DINO features [5] to measure the distance between two sets of generations. The experiment shows that edits resulting from latent encodings \hat{I}_T are characterized by higher similarity (SSIM, DINO) and lower diversity (DreamSim, LPIPS) relative to starting images I_S than the one resulting from noises I_T . At the same time, in the bottom rows of table 10,

Table 9: **Starting inversion with forward diffusion improves quality (FID) of latent interpolations.** Replacing first steps improves generations' diversity (Recall).

Inversion steps replaced by forward (% T)	DiT SLERP $_{\lambda=0.5}$		
	FID ↓	Precision ↑	Recall ↑
Noise x_T	16.61	0.799	0.473
DDIM Latent \hat{x}_T	19.68	0.795	0.415
1 (2%)	16.89	0.816	0.443
1... 2 (4%)	16.74	0.817	0.443
1... 5 (10%)	17.05	0.812	0.444
1... 10 (20%)	17.02	0.809	0.454

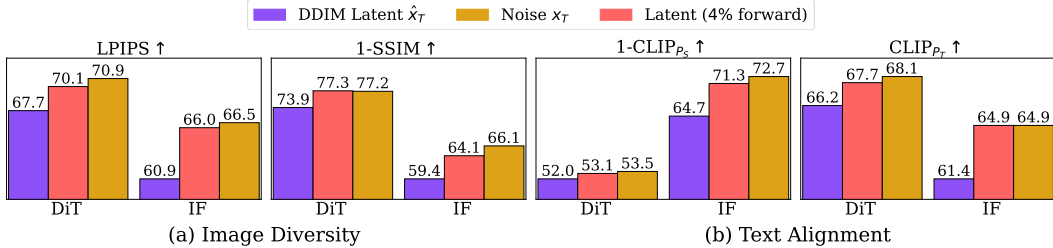


Figure 7: **Replacing first DDIM inversion steps with forward diffusion improves editions’ pixel diversity (a) and prompt-alignment (b).** For IF and DiT models, diversity of generations can be improved by leveraging the forward diffusion process in the first inversion steps, and denoising resulting latents with a different prompt. Additionally, we observe a boost in generations’ alignment to the target prompts, as indicated by the larger CLIP-T value for P_T and the smaller one for P_S . We present details of the experiment in appendix J.

we show that the correlations occurring in the latent encodings induce lower performance in text-alignment to target prompts P_T , which we measure by calculating cosine similarity between text embeddings and resulting image embeddings, both obtained with the CLIP [44] encoder. For the DiT model, our experiment indicates that generations from latents are as similar to the target prompt from the regeneration as to the source one.

Property	Metric	DiT		Deepfloyd IF	
		Noise x_T	Latent \hat{x}_T	Noise x_T	Latent \hat{x}_T
Diversity against I_S	DreamSim \uparrow	0.71 \pm 0.12	0.68 \pm 0.13	0.67 \pm 0.10	0.61 \pm 0.11
	LPIPS \uparrow	0.59 \pm 0.12	0.57 \pm 0.12	0.38 \pm 0.11	0.33 \pm 0.11
	SSIM \downarrow	0.23 \pm 0.13	0.26 \pm 0.14	0.34 \pm 0.15	0.41 \pm 0.15
	DINO \downarrow	0.17	0.22	0.34	0.42
Text alignment	CLIP-T (P_S) \downarrow	0.465	0.480	0.273	0.649
	CLIP-T (P_T) \uparrow	0.689	0.568	0.353	0.614

Table 10: **Diversity of editions (generations from noise x_T and latents \hat{x}_T , conditioned on target prompt) in relation to source images I_S and their alignment with source and target prompts.** The arrows (\uparrow/\downarrow) indicate greater generation diversity and higher text alignment to the target prompt.

We further evaluate how replacing the first inversion steps with the forward diffusion affects the diversity and text alignment of generated outputs. As shown in fig. 7a, swapping the first 4% of DDIM inversion steps with forward diffusion improves the diversity of images generated from latents almost to the level of the samples from original noise. At the same time, as presented in fig. 7b, replacing the first inversion steps leads to a significant decrease in generations’ alignment to the source prompt (P_S) and an increase in similarity to the target prompt (P_T). This can also be observed in visualisations (fig. 6).

Conversely, replacing 4% of model predictions with a forward diffusion makes the process faster by around 3.9%. Although at the same time, intuitively, replacing the predicted noise with a random one should degrade reconstruction quality, recent studies [6, 33, 30, 10] have shown that the backward diffusion final steps do not contribute additional generative information, functioning instead as a data-agnostic denoising process. Therefore, substituting noise only in the initial steps of the inversion (e.g., the first 4%) allows us to enhance the quality of the latent representations while maintaining a reconstruction error at the level of the standard DDIM inversion. This means that the error between the ground truth prediction and DDIM approximation (eq. (4)) is comparable to the error introduced with random Gaussian noise of the adjusted magnitude. Additionally, as presented in appendix K, our approach enables stochastic image editing, producing diverse manipulations of the same image.

On top of the experiments presented in this section, in the appendices, we provide additional studies comparing noise-to-image and latent-to-image mappings (appendix L) and the relation between noise and samples during training (appendix M).

5 Conclusions

In this work, we analyze how errors introduced by the DDIM inversion algorithm influence the properties of latent image representations. Our findings reveal that the inverted latents exhibit systematic deviations from a Gaussian distribution, particularly in regions corresponding to smooth image surfaces. We trace this effect to the higher inversion error in these areas, which predominantly arises during the early noising steps. This discrepancy leads to practical limitations such as reduced diversity and lower text alignment to the conditioning prompts, or worse quality interpolation and editing in situations where latents are used as a starting point of the diffusion process. To mitigate this issue, we introduce a simple yet effective solution, where we decorrelate latents by replacing the initial steps of the inversion procedure with forward diffusion. Our approach significantly improves the quality of samples in the practical use cases of DDIM inversion.

References

- [1] E. Bodin, A. I. Stere, D. D. Margineantu, C. H. Ek, and H. Moss. Linear combinations of latents in generative models: subspaces and beyond. In *The Thirteenth International Conference on Learning Representations*, 2025. URL <https://openreview.net/forum?id=n5PrId7pk5>.
- [2] M. Brack, F. Friedrich, K. Kornmeier, L. Tsaban, P. Schramowski, K. Kersting, and A. Passos. Ledits++: Limitless image editing using text-to-image models. *CVPR*, 2024.
- [3] D. Ceylan, C.-H. P. Huang, and N. J. Mitra. Pix2video: Video editing using image diffusion. In *Proceedings of the IEEE/CVF International Conference on Computer Vision (ICCV)*, pages 23206–23217, October 2023. URL https://openaccess.thecvf.com/content/ICCV2023/html/Ceylan_Pix2Video_Video_Editing_using_Image_Diffusion_ICCV_2023_paper.html.
- [4] H. Cho, J. Lee, S. B. Kim, T.-H. Oh, and Y. Jeong. Noise map guidance: Inversion with spatial context for real image editing. In *The Twelfth International Conference on Learning Representations*, 2024. URL <https://openreview.net/forum?id=mhgm0IXtHw>.
- [5] T. Darcet, M. Oquab, J. Mairal, and P. Bojanowski. Vision transformers need registers. In *The Twelfth International Conference on Learning Representations, ICLR 2024, Vienna, Austria, May 7-11, 2024*. OpenReview.net, 2024. URL <https://openreview.net/forum?id=2dn03LLiJ1>.
- [6] K. Deja, A. Kuzina, T. Trzcinski, and J. Tomczak. On analyzing generative and denoising capabilities of diffusion-based deep generative models. *Advances in Neural Information Processing Systems*, 35:26218–26229, 2022.
- [7] K. Deja, G. Tinchev, M. Czarnowska, M. Cotescu, and J. Droppo. Diffusion-based accent modelling in speech synthesis. In *Interspeech 2023*, 2023. URL <https://www.amazon.science/publications/diffusion-based-accent-modelling-in-speech-synthesis>.
- [8] P. Dhariwal and A. Nichol. Diffusion models beat GANs on image synthesis. *Advances in Neural Information Processing Systems*, 34, 2021.
- [9] W. Dong, S. Xue, X. Duan, and S. Han. Prompt tuning inversion for text-driven image editing using diffusion models. In *Proceedings of the IEEE/CVF International Conference on Computer Vision*, pages 7430–7440, 2023.
- [10] B. Fesl, B. Böck, F. Strasser, M. Baur, M. Joham, and W. Utschick. On the asymptotic mean square error optimality of diffusion models. *arXiv preprint arXiv:2403.02957*, 2024.
- [11] S. Fu, N. Tamir, S. Sundaram, L. Chai, R. Zhang, T. Dekel, and P. Isola. Dreamsim: Learning new dimensions of human visual similarity using synthetic data. In *Advances in Neural Information Processing Systems*, volume 36, pages 50742–50768, 2023.
- [12] D. Garibi, O. Patashnik, A. Voynov, H. Averbuch-Elor, and D. Cohen-Or. Renoise: Real image inversion through iterative noising. *arXiv preprint arXiv: 2403.14602*, 2024. URL <https://arxiv.org/abs/2403.14602v1>.
- [13] L. Han, S. Wen, Q. Chen, Z. Zhang, K. Song, M. Ren, R. Gao, A. Stathopoulos, X. He, Y. Chen, et al. Proxedit: Improving tuning-free real image editing with proximal guidance. In *Proceedings of the IEEE/CVF Winter Conference on Applications of Computer Vision*, pages 4291–4301, 2024.
- [14] A. Hertz, R. Mokady, J. Tenenbaum, K. Aberman, Y. Pritch, and D. Cohen-Or. Prompt-to-prompt image editing with cross attention control. *International Conference on Learning Representations*, 2022. doi: 10.48550/arXiv.2208.01626.
- [15] J. Ho and T. Salimans. Classifier-free diffusion guidance. In *NeurIPS 2021 Workshop on Deep Generative Models and Downstream Applications*, 2021. URL <https://openreview.net/forum?id=qw8AKxfYbI>.

- [16] J. Ho, A. Jain, and P. Abbeel. Denoising diffusion probabilistic models. In H. Larochelle, M. Ranzato, R. Hadsell, M. Balcan, and H. Lin, editors, *Advances in Neural Information Processing Systems*, volume 33, pages 6840–6851. Curran Associates, Inc., 2020. URL https://proceedings.neurips.cc/paper_files/paper/2020/file/4c5bcfec8584af0d967f1ab10179ca4b-Paper.pdf.
- [17] J. Ho, W. Chan, C. Saharia, J. Whang, R. Gao, A. Gritsenko, D. P. Kingma, B. Poole, M. Norouzi, D. J. Fleet, et al. Imagen video: High definition video generation with diffusion models. *arXiv preprint arXiv:2210.02303*, 2022.
- [18] S. Hong, K. Lee, S. Y. Jeon, H. Bae, and S. Y. Chun. On exact inversion of dpm-solvers. In *Proceedings of the IEEE/CVF Conference on Computer Vision and Pattern Recognition*, pages 7069–7078, 2024.
- [19] I. Huberman-Spiegelglas, V. Kulikov, and T. Michaeli. An edit friendly ddpmm noise space: Inversion and manipulations. In *Proceedings of the IEEE/CVF Conference on Computer Vision and Pattern Recognition*, pages 12469–12478, 2024.
- [20] X. Ju, A. Zeng, Y. Bian, S. Liu, and Q. Xu. Pnp inversion: Boosting diffusion-based editing with 3 lines of code. In *The Twelfth International Conference on Learning Representations*, 2024. URL <https://openreview.net/forum?id=FoMZ41jhVw>.
- [21] Z. Kadkhodaie, F. Guth, E. P. Simoncelli, and S. Mallat. Generalization in diffusion models arises from geometry-adaptive harmonic representations. In *The Twelfth International Conference on Learning Representations, ICLR 2024, Vienna, Austria, May 7-11, 2024*. OpenReview.net, 2024. URL <https://openreview.net/forum?id=ANvmVS2Yr0>.
- [22] V. Khrulkov and I. Oseledets. Understanding ddpmm latent codes through optimal transport. *International Conference on Learning Representations*, 2022. URL <https://arxiv.org/abs/2202.07477v2>.
- [23] G. Kim, T. Kwon, and J. C. Ye. Diffusionclip: Text-guided diffusion models for robust image manipulation. In *Proceedings of the IEEE/CVF Conference on Computer Vision and Pattern Recognition (CVPR)*, pages 2426–2435, June 2022.
- [24] G. Kim, T. Kwon, and J. C. Ye. Diffusionclip: Text-guided diffusion models for robust image manipulation. In *Proceedings of the IEEE/CVF conference on computer vision and pattern recognition*, pages 2426–2435, 2022.
- [25] Y.-H. Kim and E. Milman. A generalization of caffarelli’s contraction theorem via (reverse) heat flow. *Mathematische Annalen*, 2011. doi: 10.1007/s00208-011-0749-x.
- [26] D. P. Kingma and M. Welling. Auto-Encoding Variational Bayes. In *International Conference on Learning Representations*, 2014.
- [27] T. Kynkäänniemi, T. Karras, S. Laine, J. Lehtinen, and T. Aila. Improved precision and recall metric for assessing generative models. *Advances in neural information processing systems*, 32, 2019.
- [28] H. Lavenant and F. Santambrogio. The flow map of the fokker–planck equation does not provide optimal transport. *Applied Mathematics Letters*, 133:108225, 2022. ISSN 0893-9659. doi: <https://doi.org/10.1016/j.aml.2022.108225>. URL <https://www.sciencedirect.com/science/article/pii/S089396592200180X>.
- [29] S. Lee, B. Kim, and J. C. Ye. Minimizing trajectory curvature of ode-based generative models. In *International Conference on Machine Learning*, pages 18957–18973. PMLR, 2023.
- [30] M. Li and S. Chen. Critical windows: non-asymptotic theory for feature emergence in diffusion models. *arXiv preprint arXiv:2403.01633*, 2024.
- [31] X. Li, H. Tu, M. Hui, Z. Wang, B. Zhao, J. Xiao, S. Ren, J. Mei, Q. Liu, H. Zheng, Y. Zhou, and C. Xie. What if we recaption billions of web images with llama-3? *arXiv preprint arXiv:2406.12345*, 2024.

- [32] H. Lin, M. Wang, J. Wang, W. An, Y. Chen, Y. Liu, F. Tian, G. Dai, J. Wang, and Q. Wang. Schedule your edit: A simple yet effective diffusion noise schedule for image editing. *Neural Information Processing Systems*, 2024. doi: 10.48550/arXiv.2410.18756.
- [33] H. Liu, W. Zhang, J. Xie, F. Faccio, M. Xu, T. Xiang, M. Z. Shou, J.-M. Perez-Rua, and J. Schmidhuber. Faster diffusion via temporal attention decomposition. *arXiv preprint arXiv:2404.02747*, 2024.
- [34] J. Liu, C. Li, Y. Ren, F. Chen, and Z. Zhao. Diffsinger: Singing voice synthesis via shallow diffusion mechanism. *AAAI Conference on Artificial Intelligence*, 2021. doi: 10.1609/aaai.v36i10.21350.
- [35] B. Meiri, D. Samuel, N. Darshan, G. Chechik, S. Avidan, and R. Ben-Ari. Fixed-point inversion for text-to-image diffusion models. *arXiv preprint arXiv:2312.12540*, 2023.
- [36] C. Meng, Y. He, Y. Song, J. Song, J. Wu, J. Zhu, and S. Ermon. Sdedit: Guided image synthesis and editing with stochastic differential equations. In *The Tenth International Conference on Learning Representations, ICLR 2022, Virtual Event, April 25-29, 2022*. OpenReview.net, 2022. URL https://openreview.net/forum?id=aBsCjcPu_tE.
- [37] D. Miyake, A. Iohara, Y. Saito, and T. Tanaka. Negative-prompt inversion: Fast image inversion for editing with text-guided diffusion models. *arXiv preprint arXiv: 2305.16807*, 2023.
- [38] R. Mokady, A. Hertz, K. Aberman, Y. Pritch, and D. Cohen-Or. Null-text inversion for editing real images using guided diffusion models. In *Proceedings of the IEEE/CVF Conference on Computer Vision and Pattern Recognition (CVPR)*, pages 6038–6047, June 2023. URL https://openaccess.thecvf.com/content/CVPR2023/html/Mokady_NULL-Text_Inversion_for_Editing_Real_Images_Using_Guided_Diffusion_Models_CVPR_2023_paper.html.
- [39] A. Q. Nichol and P. Dhariwal. Improved denoising diffusion probabilistic models. In *International conference on machine learning*, pages 8162–8171. PMLR, 2021.
- [40] Z. Pan, R. Gherardi, X. Xie, and S. Huang. Effective real image editing with accelerated iterative diffusion inversion. In *Proceedings of the IEEE/CVF International Conference on Computer Vision (ICCV)*, pages 15912–15921, October 2023.
- [41] G. Parmar, K. Kumar Singh, R. Zhang, Y. Li, J. Lu, and J.-Y. Zhu. Zero-shot image-to-image translation. In *ACM SIGGRAPH 2023 Conference Proceedings*, pages 1–11, 2023.
- [42] W. Peebles and S. Xie. Scalable diffusion models with transformers. In *Proceedings of the IEEE/CVF International Conference on Computer Vision (ICCV)*, pages 4195–4205, October 2023.
- [43] V. Popov, I. Vovk, V. Gogoryan, T. Sadekova, and M. Kudinov. Grad-tts: A diffusion probabilistic model for text-to-speech. In *International Conference on Machine Learning*, pages 8599–8608. PMLR, 2021.
- [44] A. Radford, J. W. Kim, C. Hallacy, A. Ramesh, G. Goh, S. Agarwal, G. Sastry, A. Askell, P. Mishkin, J. Clark, G. Krueger, and I. Sutskever. Learning transferable visual models from natural language supervision. In *ICML*, 2021.
- [45] R. Rombach, A. Blattmann, D. Lorenz, P. Esser, and B. Ommer. High-resolution image synthesis with latent diffusion models. *Computer Vision and Pattern Recognition*, 2021. doi: 10.1109/CVPR52688.2022.01042.
- [46] L. Rout, Y. Chen, N. Ruiz, C. Caramanis, S. Shakkottai, and W.-S. Chu. Semantic image inversion and editing using rectified stochastic differential equations. In *The Thirteenth International Conference on Learning Representations*, 2025. URL <https://openreview.net/forum?id=Hu0FS0SEyS>.
- [47] D. Samuel, R. Ben-Ari, N. Darshan, H. Maron, and G. Chechik. Norm-guided latent space exploration for text-to-image generation. *Advances in Neural Information Processing Systems*, 36:57863–57875, 2023.

- [48] K. Shoemake. Animating rotation with quaternion curves. In *Proceedings of the 12th Annual Conference on Computer Graphics and Interactive Techniques*, SIGGRAPH '85, page 245–254, New York, NY, USA, 1985. Association for Computing Machinery. ISBN 0897911660. doi: 10.1145/325334.325242. URL <https://doi.org/10.1145/325334.325242>.
- [49] J. Sohl-Dickstein, E. Weiss, N. Maheswaranathan, and S. Ganguli. Deep unsupervised learning using nonequilibrium thermodynamics. In *International Conference on Machine Learning*, pages 2256–2265. PMLR, 2015.
- [50] J. Song, C. Meng, and S. Ermon. Denoising diffusion implicit models. *arXiv preprint arXiv:2010.02502*, 2020.
- [51] Y. Song, J. Sohl-Dickstein, D. P. Kingma, A. Kumar, S. Ermon, and B. Poole. Score-based generative modeling through stochastic differential equations. In *9th International Conference on Learning Representations, ICLR 2021, Virtual Event, Austria, May 3-7, 2021*. OpenReview.net, 2021. URL <https://openreview.net/forum?id=PxtIG12RRHS>.
- [52] StabilityAI. DeepFloyd IF: a novel state-of-the-art open-source text-to-image model with a high degree of photorealism and language understanding. <https://github.com/deep-floyd/IF>, 2023. Retrieved on 2023-04-17.
- [53] X. Su, J. Song, C. Meng, and S. Ermon. Dual diffusion implicit bridges for image-to-image translation. *International Conference on Learning Representations*, 2022. doi: 10.48550/arXiv.2203.08382.
- [54] C. Tang, K. Wang, and J. van de Weijer. IterInv: Iterative Inversion for Pixel-Level T2I Models. In *2024 IEEE International Conference on Multimedia and Expo (ICME)*, pages 1–6, Los Alamitos, CA, USA, 2024. IEEE Computer Society. doi: 10.1109/ICME57554.2024.10687547. URL <https://doi.ieeecomputersociety.org/10.1109/ICME57554.2024.10687547>.
- [55] B. Wallace, A. Gokul, and N. Naik. Edict: Exact diffusion inversion via coupled transformations. In *Proceedings of the IEEE/CVF Conference on Computer Vision and Pattern Recognition*, pages 22532–22541, 2023.
- [56] F. Wang, H. Yin, Y. Dong, H. Zhu, C. Zhang, H. Zhao, H. Qian, and C. Li. Belm: Bidirectional explicit linear multi-step sampler for exact inversion in diffusion models. *Neural Information Processing Systems*, 2024. doi: 10.48550/arXiv.2410.07273.
- [57] Z. Wang, A. C. Bovik, H. R. Sheikh, and E. P. Simoncelli. Image quality assessment: from error visibility to structural similarity. *IEEE transactions on image processing*, 13(4):600–612, 2004.
- [58] G. Zhang, J. Ji, Y. Zhang, M. Yu, T. S. Jaakkola, and S. Chang. Towards coherent image inpainting using denoising diffusion implicit models. In A. Krause, E. Brunskill, K. Cho, B. Engelhardt, S. Sabato, and J. Scarlett, editors, *International Conference on Machine Learning, ICML 2023, 23-29 July 2023, Honolulu, Hawaii, USA*, volume 202 of *Proceedings of Machine Learning Research*, pages 41164–41193. PMLR, 2023. URL <https://proceedings.mlr.press/v202/zhang23q.html>.
- [59] H. Zhang, J. Zhou, Y. Lu, M. Guo, L. Shen, and Q. Qu. The emergence of reproducibility and consistency in diffusion models, 2024. URL <https://openreview.net/forum?id=UkLSvLqi07>.
- [60] K. Zhang, Y. Zhou, X. Xu, B. Dai, and X. Pan. Diffmorpher: Unleashing the capability of diffusion models for image morphing. In *Proceedings of the IEEE/CVF Conference on Computer Vision and Pattern Recognition*, pages 7912–7921, 2024.
- [61] R. Zhang, P. Isola, A. A. Efros, E. Shechtman, and O. Wang. The unreasonable effectiveness of deep features as a perceptual metric. In *CVPR*, 2018.
- [62] Y. Zhang, J. Xing, E. Lo, and J. Jia. Real-world image variation by aligning diffusion inversion chain. In A. Oh, T. Naumann, A. Globerson, K. Saenko, M. Hardt, and S. Levine, editors, *Advances in Neural Information Processing Systems*, volume 36, pages 30641–30661. Curran Associates, Inc., 2023. URL https://proceedings.neurips.cc/paper_files/paper/2023/file/61960fdafa4d4e95fa1c1f6e64bfe8bc-Paper-Conference.pdf.

- [63] P. Zheng, Y. Zhang, Z. Fang, T. Liu, D. Lian, and B. Han. Noisediffusion: Correcting noise for image interpolation with diffusion models beyond spherical linear interpolation. In *The Twelfth International Conference on Learning Representations*, 2024.

Appendix

Contents

A	Limitations	16
B	Broader impact	16
C	Compute resources	16
D	Approximation error in DDIM Inversion	17
E	Correlations vs. inversion steps	18
F	Most probable triangles	19
F.1	Methodology	19
F.2	Impact of T on noise-image-latent triangles	20
F.3	Example histograms	20
G	Plain surface thresholding	21
H	Calculating inversion error	22
I	Pseudocode for DDIM Inversion with Forward Diffusion	22
J	Details on diversity and alignment of edition	23
K	Stochastic editing of real images	24
L	Noise-to-image mapping	25
L.1	Smallest l_2 mapping	25
L.2	Asymmetry of Noise-to-Image mapping	26
M	On Noise-Image-Latent relations during diffusion training	27
M.1	Spatial relations of noise and latents over training time	27
M.2	Image-to-noise distance mapping over training time	27
M.3	Image alignment over training time	28
N	Additional results	31
N.1	Failure cases	31
N.2	Interpolation	32

In the Appendix we first outline the limitations (**A**) of our experiments, discuss the broader impact (**B**) of the introduced method, and list the computational resources (**C**) used. We then describe, in detail, the DDIM approximation error (**D**), which effects we study in this work and the consequences it has across varying numbers of sampling steps (**E**).

Next, we describe our experimental procedures: measuring the angles of the noise–image–latent triangle (**F**), identifying plain-regions pixels (**G**) in the image, and computing the inversion error (**H**). In section **I**, we provide the full pseudocode for the proposed algorithm.

We demonstrate how the technique enhances image diversity and prompt alignment (**J**) and how it enables stochastic editing of real images (**K**). Finally, we compare Gaussian noise and DDIM latents in their mappings to images (**L**) and track how these relationships evolve during diffusion training (**M**). In section **N**, we include additional qualitative results for the experiments, especially when introduced method might fail, and how it performs in the task of image interpolation.

A Limitations

In this work, we analyzed the relation between the random noise, image generations and their latent encodings obtained through DDIM Inversion. While our studies focused on DDIM approximation error from Song et al. [50], there exist other solvers and inversion methods, as described in section 2, bringing their own advantages and limitations. The error of DDIM inversion strongly depends on the number of steps with which it is performed. In particular, performing the process very granularly, e.g., using $T = 1000$ steps, can result in strong suppression of the correlation. Nevertheless, the default number of steps we have chosen, i.e., 100, is, according to previous works [18, 12, 24], a practical choice as a good balance between the reconstruction error and the speed of the algorithm. In appendix E, we present that the latents exhibit correlations when using more sampling steps.

The observations from our analytical experiments (correlations in table 2, angles in table 3, variance in table 4, interpolations in fig. 5) generalize well to all tested diffusion models, but are less evident in the LDM model trained on the CelebA-HQ images. We attribute this exemption to the specificity of the dataset on which the model was trained - photos with centered human faces, usually with uniform backgrounds. We believe that, unlike models trained on a larger number of concepts, the process of generating faces with uniform backgrounds is more stable and introduces little detail in subsequent steps, making the difference in approximation error for plain and non-plain areas less significant.

As mentioned in section 2, the DDIM inversion error can be detrimental when using a small number of steps. Even though the solution proposed in this work (involving forward diffusion in first inversion steps) drastically removes correlations in latents and, thus, improves image interpolation and editing, it does not improve the numerical inversion error resulting from using small number of steps. In our experiments with 50 steps that are commonly used for edition, we show no significant drawbacks. However, in the extreme cases, using our method in even a single step, might result in the loss of information necessary for correct image reconstruction, hence it may be less preferred than standard DDIM inversion in some cases. In appendix N.1, we present failure cases for introduced solution.

B Broader impact

As our work is mostly analytical, we do not provide new technologies that might have a significant societal impact. However, our solution for improving the accuracy of DDIM inversion has potential implications that extend beyond technical advancements in diffusion models. As our approach enables more precise image editing it could be misused to advance image manipulation techniques. The enhanced interpolation quality could make synthetic content more convincing and harder to detect.

C Compute resources

For the experiments, we used a scientific cluster consisting of 110 nodes with CrayOS operating system. Each node is powered by 288 CPU cores, stemming from 4 NVIDIA Grace processors, each with 72 cores and a clock speed of 3.1 GHz. The nodes are equipped with substantial memory, featuring 480 GB of RAM per node. For GPU acceleration, each node in the cluster consists of 4 NVIDIA GH200 96GB GPUs with 120 GB of RAM and 72 CPUs per GPU.

Almost all of the experiments we perform are based on performing a sampling process using a diffusion model from noise, performing DDIM inversion and, possibly, image reconstruction from the latent, where each of these processes takes the same number of steps, hence the same number of GPU-hours on average. As our experiments differ in terms of number of sampling steps and images to generate, we provide average GPU time **per one sampling step** per batch (with B denoting batch size) for each model as following: ADM-32 ($B = 256$): 0.054s, ADM-64 ($B = 128$): 0.093s, ADM-256 ($B = 64$): 0.901s, LDM ($B = 128$): 0.273s, DiT ($B = 128$): 0.104s, IF ($B = 64$): 0.609s. Note that some experiments, such as analyzing inversion approximation errors per step (fig. 4) or sampling from noise interpolations (fig. 5), involves performing the procedures several times.

Taking into consideration all the experiments described in the main text of this work, fully reproducing them takes roughly 95 GPU hours. However, considering the prototyping time, preliminary and failed experiments, as well as the fact that most of the experiments must be performed sequentially (e.g., inversion after image generation, image reconstruction after inversion), the overall execution time of the entire research project is multiple times longer.

D Approximation error in DDIM Inversion

Denoising Diffusion Probabilistic Models (DDPMs [16]) generate samples by reversing the forward diffusion process, modeled as a Markov Chain, where a clean image x_0 is progressively transformed to white Gaussian noise x_T in T diffusion steps. A partially noised image x_t , which serves as an intermediate object in this process, is expressed as $x_t = \sqrt{\bar{\alpha}_t}x_0 + \sqrt{1 - \bar{\alpha}_t}\epsilon_t$ where $\bar{\alpha}_t = \prod_{s=1}^t \alpha_s$, $\alpha_t = 1 - \beta_t$, $\epsilon_t \sim \mathcal{N}(0, \mathcal{I})$, and $\{\beta_t\}_{t=1}^T$ is a variance schedule, controlling how much of the noise is contained in the image at the specific step t .

To enable sampling clean images from clean Gaussian noises, the neural network ϵ_θ is trained to predict the noise added to a clean image x_0 for a given intermediate image x_t . Such a trained model is further utilized in the backward diffusion process by iteratively transferring a more noisy image (x_t) to the less noisy one (x_{t-1}) as

$$x_{t-1} = \frac{1}{\sqrt{\alpha_t}} \left(x_t - \frac{\beta_t}{\sqrt{1 - \bar{\alpha}_t}} \epsilon_\theta^{(t)}(x_t) \right) + \sigma_t z, \quad (6)$$

with $z \sim \mathcal{N}(0, \mathcal{I})$ being a noise portion added back for denoising controlled by $\sigma_t = \sqrt{\beta_t(1 - \bar{\alpha}_{t-1})/(1 - \bar{\alpha}_t)}$.

Song et al. [50] reformulate the diffusion process as a non-Markovian, which leads to a speed-up of the sampling process. While previously obtaining a less noisy image at x_t required all past denoising steps from T till $(t + 1)$, this approach allows skipping some steps during sampling. More precisely, the backward diffusion process is defined as a combination of predictions of image x_0 , next denoising step x_t , and random noise (with $\sigma_t = \eta\sqrt{\beta_t(1 - \bar{\alpha}_{t-1})/(1 - \bar{\alpha}_t)}$ and $z_t \sim \mathcal{N}(0, \mathcal{I})$):

$$x_{t-1} = \sqrt{\bar{\alpha}_{t-1}} \left(\frac{x_t - \sqrt{1 - \bar{\alpha}_t} \epsilon_\theta^{(t)}(x_t)}{\sqrt{\bar{\alpha}_t}} \right) + \sqrt{1 - \bar{\alpha}_{t-1} - \sigma_t^2} \cdot \epsilon_\theta^{(t)}(x_t) + \sigma_t z_t. \quad (7)$$

While setting $\eta = 1$ makes eq. (7) equivalent to eq. (6), leading to a Markovian probabilistic diffusion model, setting $\eta = 0$ removes the random component from the equation, making it a Denoising Diffusion Implicit Model (DDIM), which prominent ability is to perform a deterministic mapping from given noise (x_T) to image (x_0). One of the potential benefits of implicit models is the possibility of reversing the backward diffusion process to transfer images back to the original noise. Operating in such a space by modifying resulting inversions unlocks numerous image manipulation capabilities, i.a., image editing [14, 38, 19, 41, 46, 37, 2, 54, 18, 55, 35, 12, 40, 9], image interpolation [63, 60, 47, 8], or stroke-to-image synthesis [36, 46]. The inversion process can be derived from eq. (7), leading to the formula for transferring a less noisy image x_{t-1} to a more noisy one x_t :

$$x_t = \sqrt{\alpha_t}x_{t-1} + (\sqrt{1 - \bar{\alpha}_t} - \sqrt{\alpha_t - \bar{\alpha}_t}) \cdot \epsilon_\theta^{(t)}(x_t) \quad (8)$$

Unfortunately, a perfect image-to-noise inversion is infeasible. Due to circular dependency on x_t within eq. (8), Dhariwal and Nichol [8] propose to approximate this equation by assuming that the model’s prediction in t -th step is locally equivalent to the decision in $(t - 1)$ -th step $\epsilon_\theta^{(t)}(x_t) \approx \epsilon_\theta^{(t)}(x_{t-1})$. The inverted trajectory is determined in multiple steps. Hence, the error propagates further away from the image, leading to the latents that deviate from the starting noise. This flaw is presented in fig. 8.

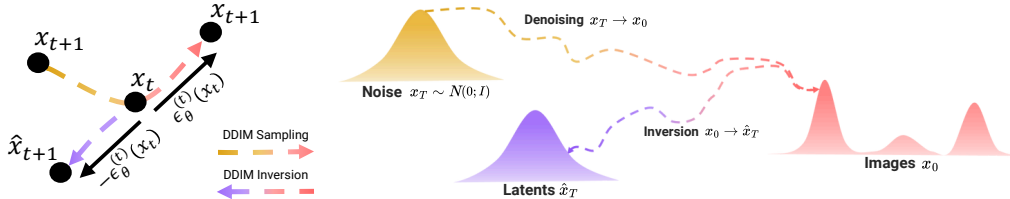


Figure 8: The DDIM inversion error, derived from approximating DM’s prediction in step t with the $(t + 1)$ output (left), propagates with the next inversion steps, leading to a distribution of latents \hat{x}^T that deviates significantly from the expected noise distribution x^T (right).

E Correlations vs. inversion steps

In this work, for the inversion process, we leverage the DDIM sampler with either $T = 50$ or $T = 100$ sampling steps. This choice aligns with prior works [18, 12, 24] in image edition domain, where the authors used from 50 up to 200 inversion steps as a proper balance between reconstruction quality and short algorithm runtime.

However, as described in Hong et al. [18], the naïve DDIM inversion procedure [50] can be reinterpreted as solving the forward diffusion ordinary differential equation (ODE) in reverse order (along the time axis) with Euler method. With this reformulation, the inversion is correct under the assumption that, with dt being step size, noise predictions in t and $t + dt$ steps are almost exact, thus works only when performing with many iterations.

Since the presence of image structures in DDIM latents can depend on the number of steps with which the inversion is performed, in table 11 we show for ADM-64, DiT, and IF models that the observations we presented in this work generalize to cases where the number of inversion steps is several times greater (i.e., $T = 1000$, as performed during the training). Additionally, in fig. 9 we show qualitatively by plotting the absolute error between starting Gaussian noise and DDIM latents, that also for a large number of steps, the uniform areas on the image contribute more significantly to overall inversion error.

Object	Model		
	ADM-64	DiT	IF
Noise x_T (baseline)	0.039 \pm .00	0.039 \pm .00	0.039 \pm .00
DDIM Latent $\hat{x}_{T=10}$	0.416 \pm .03	0.297 \pm .01	0.783 \pm .01
DDIM Latent $\hat{x}_{T=25}$	0.242 \pm .02	0.203 \pm .02	0.698 \pm .02
DDIM Latent $\hat{x}_{T=50}$	0.177 \pm .02	0.144 \pm .02	0.608 \pm .02
DDIM Latent $\hat{x}_{T=100}$	0.133 \pm .01	0.106 \pm .02	0.500 \pm .02
DDIM Latent $\hat{x}_{T=250}$	0.108 \pm .01	0.078 \pm .01	0.366 \pm .02
DDIM Latent $\hat{x}_{T=500}$	0.100 \pm .01	0.069 \pm .01	0.294 \pm .02
DDIM Latent $\hat{x}_{T=1000}$	0.095 \pm .01	0.065 \pm .01	0.249 \pm .02

Table 11: **Latent encodings resulting from the DDIM Inversion exhibit correlations, even when the procedure is performed with a lot of steps.** By dividing latent encodings into 8×8 patches and calculating inside the mean of top-20 absolute Pearson correlation coefficients, we show that DDIM latents are correlated substantially higher than Gaussian noise, even when using $T = 1000$ inversion steps.

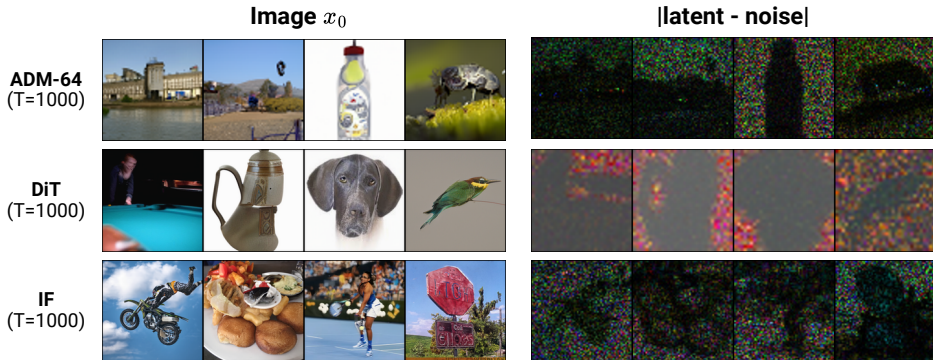


Figure 9: **Approximation errors in DDIM inversion are significantly higher for plain image surfaces than for the rest of the image.** Even when using $T = 1000$ steps, we observe image structures in resulting latents, which can be attributed to less diverse outputs for uniform image regions.

F Most probable triangles

In section 3.2, we analyze where the latent encodings are distributed in relation to the initial noise and generated samples. In this section, we describe the methodology for obtaining such triangles, as well as investigate how those relations change depending on a number of diffusion steps T .

F.1 Methodology

First, we determine the vectors going from each vertex to the other vertices of the noise-sample-latent ($\mathbf{x}_T - \mathbf{x}_0 - \hat{\mathbf{x}}_T$) triangle. For sample \mathbf{x}_0 , we obtain a vector leading to noise $\overrightarrow{\mathbf{x}_0 \mathbf{x}_T} = \mathbf{x}_T - \mathbf{x}_0$ and to latent $\overrightarrow{\mathbf{x}_0 \hat{\mathbf{x}}_T} = \hat{\mathbf{x}}_T - \mathbf{x}_0$, and calculate the angle between them using cosine similarity as

$$\angle \mathbf{x}_0 = \arccos \frac{\overrightarrow{\mathbf{x}_0 \mathbf{x}_T} \cdot \overrightarrow{\mathbf{x}_0 \hat{\mathbf{x}}_T}}{\|\overrightarrow{\mathbf{x}_0 \mathbf{x}_T}\| \|\overrightarrow{\mathbf{x}_0 \hat{\mathbf{x}}_T}\|}, \quad (9)$$

and convert resulting radians to degrees. Similarly, we obtain the angle next to the noise $\angle \mathbf{x}_T$ and latent $\angle \hat{\mathbf{x}}_T$.

Next, we determine histograms for each angle, approximating the probability density function for every angle ($p_{\angle \mathbf{x}_T}, p_{\angle \mathbf{x}_0}, p_{\angle \hat{\mathbf{x}}_T}$) binned up to the precision of one degree, see fig. 11. Finally, for all angles triples candidates (where $\angle \mathbf{x}_T + \angle \mathbf{x}_0 + \angle \hat{\mathbf{x}}_T = 180^\circ$), we calculate the probability of a triangle as the product of the probabilities and choose the triplet maximizing such joint probability:

$$\operatorname{argmax}_{(\angle \mathbf{x}_T, \angle \mathbf{x}_0, \angle \hat{\mathbf{x}}_T)} p_{\angle \mathbf{x}_T} \cdot p_{\angle \mathbf{x}_0} \cdot p_{\angle \hat{\mathbf{x}}_T}. \quad (10)$$

In fig. 10, we provide example triangles for ADM-32 (a), ADM-256 (b), and LDM (c), which we calculate using $N = 1000$ images with $T = 100$ diffusion steps.

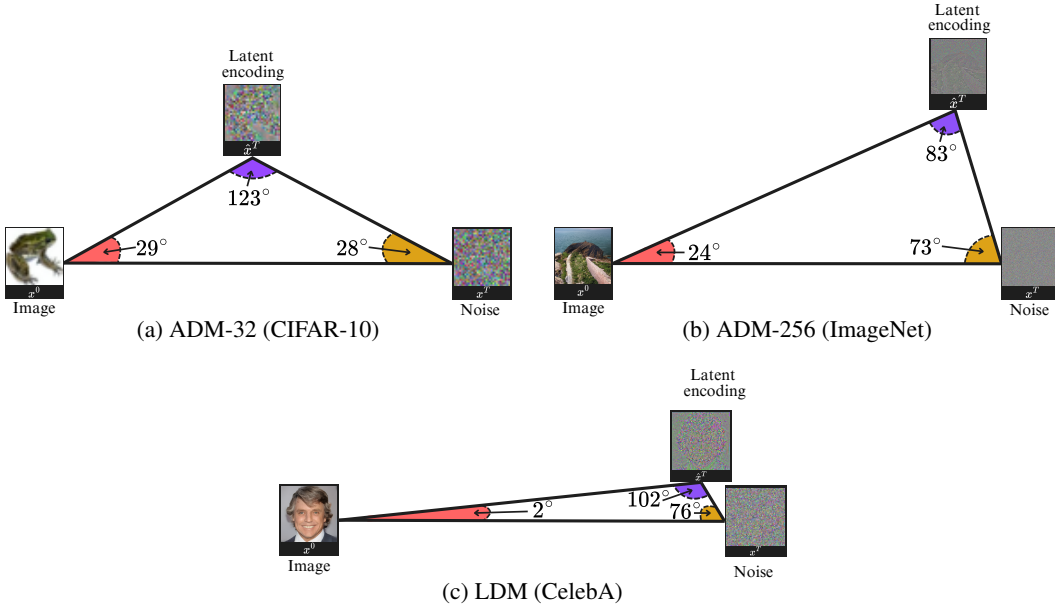


Figure 10: **Most probable triangles formed from random Gaussian noise (\mathbf{x}_T), the images (\mathbf{x}_0) generated, and latents ($\hat{\mathbf{x}}_T$) recovered with DDIM Inversion procedure.**

F.2 Impact of T on noise-image-latent triangles

In table 12 we show how the geometrical relations between Gaussian noise, generated images and DDIM latents change when sampling and inversion is done with varying T .

Model	T	$\angle \mathbf{x}_0$	$\angle \mathbf{x}_T$	$\angle \hat{\mathbf{x}}_T$
ADM 32×32	10	44	16	120
	100	29	28	123
	1000	20	45	115
ADM 64×64	10	30	31	119
	100	11	60	109
	1000	6	79	95
ADM 256×256	10	24	50	106
	100	24	73	83
	1000	23	73	84
LDM 256×256	10	23	53	104
	100	2	76	102
	1000	1	83	96
DiT 256×256	10	27	47	106
	100	4	66	110
	1000	1	80	99

Table 12: **Impact of the number of diffusion steps T on angles in the noise \mathbf{x}_T , image \mathbf{x}_0 , and latent $\hat{\mathbf{x}}_T$ triangle.** Regardless of the number of diffusion steps, latents appear between Gaussian noise and generations.

F.3 Example histograms

In fig. 11 we present histograms approximating probability density functions for noise \mathbf{x}_T , image \mathbf{x}_0 , and DDIM latent $\hat{\mathbf{x}}_T$ angles.

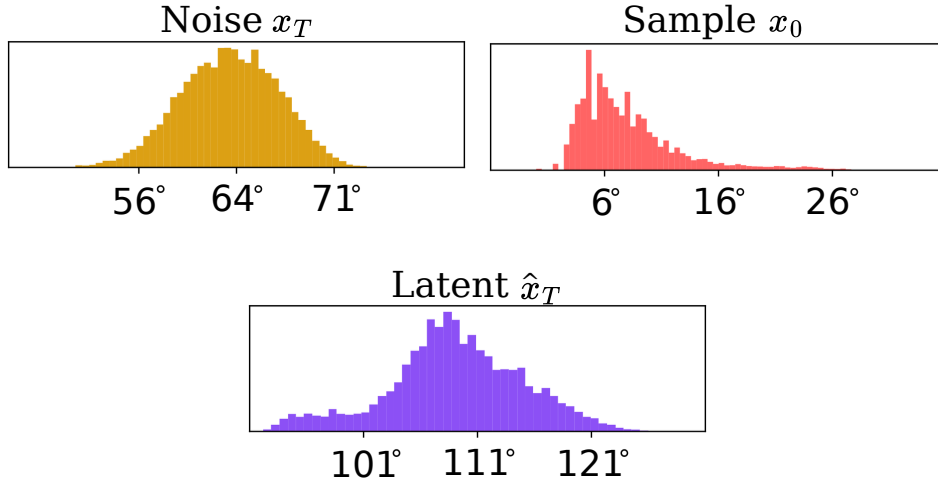


Figure 11: **Histograms approximating probability density functions of angles values for noise, sample, and latent vertices.** Example calculated for DiT model using $T = 100$ diffusion steps.

G Plain surface thresholding

During our experiments, we determine binary mask \mathcal{M} to identify pixels corresponding to the plain areas in the images. We describe this process in this section.

Let $\mathbf{I} \in \mathbb{R}^{C \times H \times W}$ be the input image. For each pixel value across every channel (c, h, w) in \mathbf{I} , we compute the absolute difference to point in the next row $D_H(c, h, w) = |I_{c,h+1,w} - I_{c,h,w}|$ and to the pixel in the next column $D_W(c, h, w) = |I_{c,h,w+1} - I_{c,h,w}|$. We obtain $D_H \in \mathbb{R}^{C \times H-1 \times W}$ and $D_W \in \mathbb{R}^{C \times H \times W-1}$, which we pad with zeros (last row for D_H and last column for D_W), making them of shape $C \times H \times W$. The difference matrix D , representing how a point varies from its neighbors, is computed as $D = (D_W + D_H)/2$.

Finally, we determine a binary mask \mathcal{M}_c per each channel c , by applying threshold τ to D as

$$\mathcal{M}_c(h, w) = \begin{cases} 1, & \text{if } D_c(h, w) < \tau \\ 0, & \text{otherwise} \end{cases} \quad (11)$$

During the experiments, we set $\tau = 0.025$.

The final mask $\mathcal{M} \in \{0, 1\}^{W \times H}$ can be derived by evaluating the logical AND across all channels for each pixel location as

$$\mathcal{M}(h, w) = \prod_c \mathcal{M}_c(h, w). \quad (12)$$

After obtaining the final mask for plain pixels, which we denote as \mathcal{M}_p , the according mask for non-plain image surfaces can be obtained by applying logical NOT to the mask as $\mathcal{M}_n = \neg \mathcal{M}_p$. In fig. 12, we present example masks determined using our methodology.

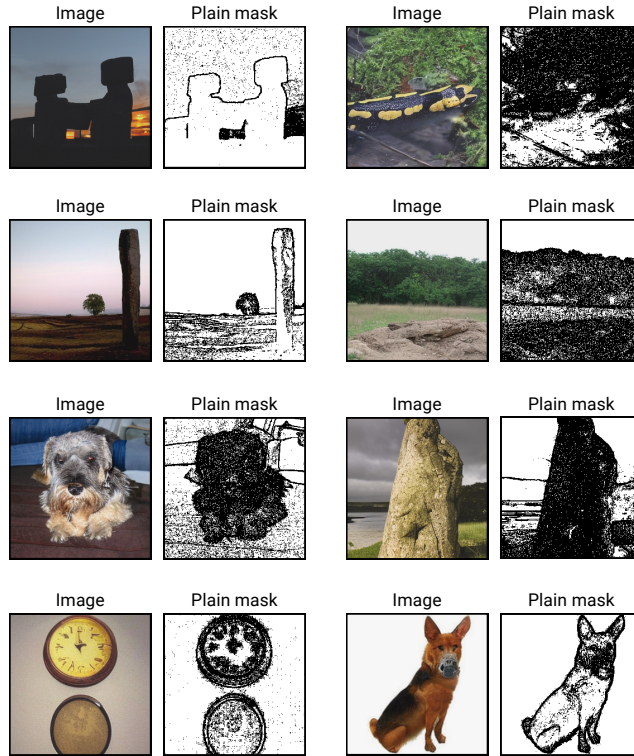


Figure 12: Examples of samples together with their masks indicating plain areas (white). Images generated using DiT model.

H Calculating inversion error

In section 3.3, we study how the inversion error differs for pixels related to plain and non-plain samples' regions and investigate it across diffusion steps. In this section, we describe the method for determining the error.

First, we generate $N = 4k$ images with $T = 50$ diffusion steps with both ADM-64 and DiT models, saving intermediate noise predictions $\{\mathcal{E}_t^S\}_{t=50\dots 1}$ during sampling. Next, we collect diffusion model outputs during the inversion process $\{\mathcal{E}_t^I\}_{t=1\dots 50}$ assuming all the previous steps were correct. While for $t = 1$, \mathcal{E}_1^I can be set to the diffusion model prediction from the first inversion step $\epsilon_\theta(x_0)$, for further steps, more advanced methodology is necessary. To this end, for each $t' = 2 \dots 50$, we map the images to latents with DDIM Inversion, replacing in $t = 1 \dots t' - 1$ the predicted noise $\epsilon_\theta(x_t)$ with the ground truth prediction \mathcal{E}_t^S from denoising process, and collect the model output for the t' step as $\mathcal{E}_{t'}^I := \epsilon_\theta(x_{t'})$. For step t , this methodology is equivalent to starting the inversion process from $(t + 1)$ denoising step and collecting the first diffusion model prediction.

In the next step, we calculate the absolute error between outputs during inversion and ground truth predictions as $\mathcal{E}_t^E = |\mathcal{E}_t^I - \mathcal{E}_t^S|$. This way, we obtain the inversion approximation error for each timestep.

Further, for the images in the dataset, we obtain binary masks \mathcal{M}_p and \mathcal{M}_n indicating, respectively, plain (p) and non-plain (n) pixels in the image, according to the procedure described in appendix G. To ensure that the level of noise that DM predicts in each step does not bias the results, we divide the absolute errors in each step by l_1 -norm of model outputs, calculated separately for each diffusion step. For plain (p) pixels, it can be described as

$$\mathcal{E}_t^{Ep} = 1/\|\mathcal{E}_t^I\|_1 \sum (\mathcal{E}_t^E \odot \mathcal{M}_p), \quad (13)$$

and adequately for non-plain (n) pixels as

$$\mathcal{E}_t^{En} = 1/\|\mathcal{E}_t^I\|_1 \sum (\mathcal{E}_t^E \odot \mathcal{M}_n). \quad (14)$$

In table 6, we present the error differences for plain and non-plain areas and how the first 10% of the diffusion steps contribute to the total inversion error. To calculate this error for plain regions in steps t_s, \dots, t_e , we sum errors for timesteps from a given interval as

$$\bar{\mathcal{E}}_{(t_s, t_e)}^{Ep} = \sum_{t'=t_s}^{t_e} \mathcal{E}_{t'}^{Ep}. \quad (15)$$

I Pseudocode for DDIM Inversion with Forward Diffusion

We present in Algorithm 1 the pseudocode for the proposed solution to the decorrelation of latent encodings by replacing the first t' inversion steps with a forward diffusion process.

Algorithm 1 Finding decorrelated DDIM latent encoding $\hat{\mathbf{x}}_T$

Require: image \mathbf{x}_0 ; diffusion model ϵ_θ ; noise schedules $\{\alpha_t\}_{t=1}^T, \{\bar{\alpha}_t\}_{t=1}^T$; number of inversion steps T ; forward-replacement timestep f

Ensure: decorrelated latent encoding $\hat{\mathbf{x}}_T$

- 1: sample $\tilde{\epsilon} \sim \mathcal{N}(0, \mathcal{I})$
 - 2: $\hat{\mathbf{x}}_f \leftarrow \sqrt{\bar{\alpha}_f} \cdot \mathbf{x}_0 + \sqrt{1 - \bar{\alpha}_f} \cdot \tilde{\epsilon}$ ▷ forward diffusion
 - 3: **for** $t \leftarrow f + 1, \dots, T$ **do**
 - 4: $\hat{\mathbf{x}}_t \leftarrow \sqrt{\alpha_t} \cdot \hat{\mathbf{x}}_{t-1} + (\sqrt{1 - \bar{\alpha}_t} - \sqrt{\alpha_t}) \cdot \epsilon_\theta^{(t)}(\hat{\mathbf{x}}_{t-1})$ ▷ DDIM Inversion step
 - 5: **end for**
 - 6: **return** $\hat{\mathbf{x}}_T$
-

J Details on diversity and alignment of edition

In this section, we provide results for measuring the diversity (against source images I_S) and alignment to conditioning prompts (source P_S and target P_T) of images generated from Gaussian noise \mathbf{x}_T , DDIM latents $\hat{\mathbf{x}}_T$, or the latents produced by our method (described in algorithm 1) with modified prompts. We use distance-based metrics (LPIPS [61], DreamSim [11]), similarity metrics (SSIM [57], DINO [5]) to measure the diversity between source (input) images and target (edited) images, as well as the similarity between embeddings produced by the CLIP [44] model to calculate the alignment between the results and prompts. The results in for introduced latent decorrelation procedure are obtained with varying percentages of the first DDIM inversion steps replaced with forward diffusion.

In table 13, we show that by selecting a small fraction of inversion steps to replace with forward diffusion (from 2% up to 6%), the resulting latents are more editable.

Inversion steps replaced by forward diff. (% T)	Diversity against I_S				CLIP Alignment	
	DreamSim \uparrow	LPIPS \uparrow	SSIM \downarrow	DINO \downarrow	$P_S \downarrow$	$P_T \uparrow$
Noise \mathbf{x}_T	0.709	0.591	0.228	0.174	0.465	0.681
DDIM Latent $\hat{\mathbf{x}}_T$	0.677	0.564	0.261	0.223	0.480	0.662
1 (2%)	0.696	0.580	0.239	0.187	0.470	0.676
1...2 (4%)	0.701	0.587	0.227	0.179	0.469	0.677
1...3 (6%)	0.705	0.594	0.216	0.173	0.468	0.678
1...5 (10%)	0.711	0.605	0.198	0.165	0.466	0.679
1...10 (20%)	0.722	0.628	0.166	0.153	0.465	0.681
1...50 (100%)	0.805	0.801	0.013	0.085	0.465	0.680

(a) Diffusion Transformer

Inversion steps replaced by forward diff. (% T)	Diversity against I_S				CLIP Alignment	
	DreamSim \uparrow	LPIPS \uparrow	SSIM \downarrow	DINO \downarrow	$P_S \downarrow$	$P_T \uparrow$
Noise (100%)	0.665	0.380	0.339	0.344	0.273	0.649
DDIM Latent $\hat{\mathbf{x}}_T$	0.609	0.328	0.406	0.416	0.353	0.614
1 (2%)	0.666	0.376	0.359	0.335	0.281	0.646
1...2 (4%)	0.660	0.369	0.359	0.351	0.287	0.649
1...3 (6%)	0.661	0.370	0.353	0.349	0.285	0.650
1...5 (10%)	0.662	0.372	0.341	0.346	0.282	0.649
1...10 (20%)	0.668	0.379	0.312	0.337	0.279	0.648
1...50 (100%)	0.733	0.521	0.004	0.272	0.274	0.649

(b) Deepfloyd IF

Table 13: **Impact of first DDIM inversion errors on diversity and text-alignment of generations from resulting latent as an input.** For both DiT (a) and IF (b) models, replacing the first inversion steps and denoising leads to more diverse generations against the source images I_S . Additionally, we show using forward diffusion in first steps improves the alignment between generation and target prompts, which the generation process is conditioned by, as indicated by the larger CLIP-T value for P_T and the smaller one for P_S .

K Stochastic editing of real images

In this work, we propose the solution for decorrelating latent encodings resulting from DDIM inversion by replacing its first steps with the forward diffusion. As presented in algorithm 1, the forward diffusion process involves sampling random Gaussian noise $\tilde{\epsilon} \sim \mathcal{N}(0, \mathcal{I})$ and interpolating it with input image. Due to the fact that, when we replace a small fraction of steps (2 – 4%), the change in image reconstruction error is insignificant, the use of different noises $\tilde{\epsilon}$ (in practice, sampled with different seeds) allows stochastic image editing, i.e. generating different manipulations of the input image, a feature not naturally available with DDIM inversion. In fig. 13, we present examples of editing **real images** from the **ImageNet-R-T12I** dataset (which we annotate using GPT-4o) with the IF model, showing various semantically correct modifications of the same image.

As preserving original image structure during editing is stated as a more difficult task for real images than the one naturally generated by diffusion model, we follow Hertz et al. [14] by, first, denoising latent encodings with source prompt (the one used during inversion), and, after 6% of the steps, using target prompt as conditioning. The examples presented in fig. 13 indicate, that our approach (1) enables stochastic editing of images and (2) enables image manipulations in plain image regions, contrary to editing with naïve DDIM latents.

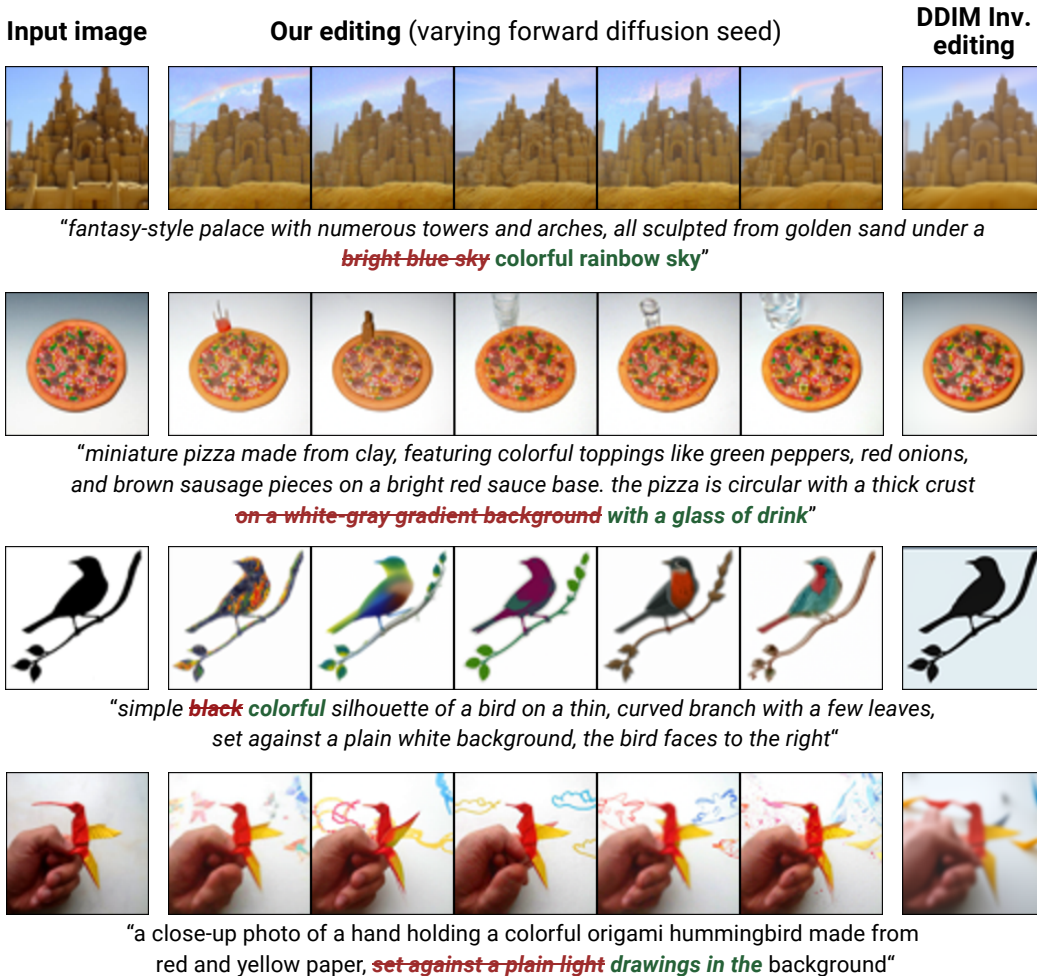


Figure 13: **Replacing first DDIM inversion steps with forward diffusion enables stochastic image editing, resulting in multiple semantically correct manipulations of same input image.** Contrary to DDIM Inversion, editing with latents produced by the solution introduced in this work, enables image manipulations in uniform input image areas.

L Noise-to-image mapping

We showcase an additional study showing the differences that occur between noise and latent encodings, from the perspective of their mapping to the images. Several works investigate interesting properties between the initial random noise and generations that result from the training objective of DDPMs and score-based models. Kadkhodaie et al. [21] show that due to inductive biases of denoising models, different DDPMs trained on similar datasets converge to almost identical solutions. This idea is further explored by Zhang et al. [59], observing that even models with different architectures converge to the same score function and, hence, the same noise-to-image mapping. Khruikov and Oseledets [22] show that diffusion models’ encoder map coincides with the optimal transport (OT) map when modeling simple distributions. However, other works [25, 28] contradict this finding.

L.1 Smallest l_2 mapping

Diffusion models converge to the same mapping between the Gaussian noise (\mathbf{x}_T) and the generated images (\mathbf{x}_0) independently on the random seed, dataset parts [21], or the model architecture [59]. We further investigate this property from the noise-sample and latent-sample mapping perspective.

In our experimental setup, we start by generating $N = 2000$ images \mathbf{x}_0 from Gaussian noise \mathbf{x}_T with a DDIM sampler and invert the images to latents $\hat{\mathbf{x}}_T$ with naïve DDIM inversion. Next, we predict resulting images for the starting noise samples ($\mathbf{x}_T \rightarrow \mathbf{x}_0$) by iterating over all the N noises, and for each of them, we calculate its pixel distances to all the N generations. For given noise, we select the image to which such l_2 -distance is the smallest. Similarly, we investigate image-to-noise ($\mathbf{x}_0 \rightarrow \mathbf{x}_T$), image-to-latent ($\mathbf{x}_0 \rightarrow \hat{\mathbf{x}}_T$) and latent-to-image ($\hat{\mathbf{x}}_T \rightarrow \mathbf{x}_0$) mappings. We calculate the distance between two objects as l_2 norm of the matrix of differences between them (with $C \times H \times W$ being the dimensions of either pixel or latent space of diffusion model) as $\|x - y\|_2 = \sqrt{\sum_i^C \sum_j^H \sum_k^W (x_{i,j,k} - y_{i,j,k})^2}$.

In table 14, we investigate the accuracy of the procedure across varying numbers of diffusion steps T for both image \leftrightarrow noise (a) and image \leftrightarrow latent (b) assignments. We show that assigning initial noise to generations ($\mathbf{x}_0 \rightarrow \mathbf{x}_T$) through the distance method can be successfully done regardless of diffusion steps. For the reverse assignment, which is noise-to-image ($\mathbf{x}_T \rightarrow \mathbf{x}_0$) mapping, we can observe high accuracy with a low number of generation timesteps ($T = 10$), but the results deteriorate quickly with the increase of this parameter. The reason for this is that greater values of T allow the generation of a broader range of images, including the ones with large plain areas of low pixel variance. When it comes to mappings between images and latents resulting from DDIM Inversion, assignment in both directions is infeasible for pixel diffusion, regardless of T .

T	ADM-32		ADM-64		ADM-256		LDM		DiT	
	$\mathbf{x}_0 \rightarrow \mathbf{x}_T$	$\mathbf{x}_T \rightarrow \mathbf{x}_0$								
10	90.3 \pm 6.3	94.0 \pm 2.6	99.4 \pm 0.0	100 \pm 0.0	100 \pm 0.0	39.2 \pm 6.2	100 \pm 0.0	100 \pm 0.0	100 \pm 0.0	93.7 \pm 7.2
100	98.9 \pm 1.2	50.4 \pm 1.9	100 \pm 0.0	59.0 \pm 7.1	100 \pm 0.0	23.2 \pm 4.8	100 \pm 0.0	100 \pm 0.0	100 \pm 0.0	90.7 \pm 10.1
1000	99.1 \pm 1.0	46.8 \pm 3.0	99.8 \pm 0.2	44.6 \pm 6.3	100 \pm 0.0	25.0 \pm 4.4	100 \pm 0.0	100 \pm 0.0	100 \pm 0.0	96.7 \pm 4.6
4000	99.1 \pm 1.0	46.4 \pm 3.0	99.5 \pm 0.3	43.3 \pm 6.7	-	-	-	-	-	-

(a) Assigning noise to the corresponding generated image ($\mathbf{x}_0 \rightarrow \mathbf{x}_T$) and vice-versa ($\mathbf{x}_T \rightarrow \mathbf{x}_0$).

T	ADM-32		ADM-64		ADM-256		LDM		DiT	
	$\mathbf{x}_0 \rightarrow \hat{\mathbf{x}}_T$	$\hat{\mathbf{x}}_T \rightarrow \mathbf{x}_0$								
10	66.4 \pm 1.7	38.2 \pm 5.1	64.4 \pm 7.1	100.0 \pm 0.0	0.7 \pm 0.2	30.8 \pm 4.3	100 \pm 0.0	100 \pm 0.0	99.8 \pm 0.6	95.1 \pm 6.4
100	16.4 \pm 6.1	33.4 \pm 2.7	8.6 \pm 9.3	57.5 \pm 7.3	4.1 \pm 1.4	23.9 \pm 5.0	100 \pm 0.0	100 \pm 0.0	99.5 \pm 1.7	90.7 \pm 10.3
1000	3.6 \pm 2.2	40.9 \pm 2.7	1.7 \pm 1.3	44.7 \pm 6.5	23.9 \pm 5.2	25.4 \pm 4.4	100 \pm 0.0	100 \pm 0.0	100.0 \pm 0.2	96.6 \pm 4.6
4000	2.8 \pm 2.2	41.9 \pm 3.0	1.9 \pm 1.4	43.5 \pm 6.5	-	-	-	-	-	-

(b) Assigning images to the resulting latent encodings ($\hat{\mathbf{x}}_T \rightarrow \mathbf{x}_0$) and vice-versa ($\mathbf{x}_0 \rightarrow \hat{\mathbf{x}}_T$).

Table 14: Accuracy of the l_2 -distance based assignment for both image \leftrightarrow noise (a) and image \leftrightarrow latent (b) mappings across varying number of diffusion steps T . For pixel DMs, only the image-to-noise ($\mathbf{x}_0 \rightarrow \mathbf{x}_T$) mapping is feasible. For the latent space models, we correctly predict assignments in all directions.

For both noise x^T and latents \hat{x}^T , their assignment to images in both directions can be successfully done when the denoising is performed in the latent space, as shown for DiT and LDM models. We hypothesize that this fact is connected with the KL regularization term that imposes a slight penalty towards a standard normal distribution $\mathcal{N}(0, I)$ on the learned latent during training [45].

L.2 Asymmetry of Noise-to-Image mapping

Results in table 14a indicate that, even though the l_2 -distance is symmetrical, the mapping cannot be done in both directions. The reason behind this is that image and noise assignments are not the same due to the one-directional many-to-one relation, e.g., there might be several noises pointing towards the same closest image.

We present examples of wrong noise-to-image ($x_T \rightarrow x_0$) assignments in fig. 14A for ADM-64. In fig. 14B, we present the singular generations that lead to incorrect noise-to-image classification (noise attractors), along with the number of noises for which they are the closest. Interestingly, in fig. 14C, we sort all the generations used in the experiment by the variance of pixels and show 8 least variant images. We observe that the set of singular generations leading to misclassification partially overlaps with lowest-variance generations. In fig. 15 we observe similar properties for experiment with ADM-32 model.

When assigning images to the initial noises, there are singular generations (with large plain areas) located close to the mean of the random Gaussian noise in the set of generated images. Such generations tend to be the closest (in l_2 -distance) for the majority of the noises in our experiments.

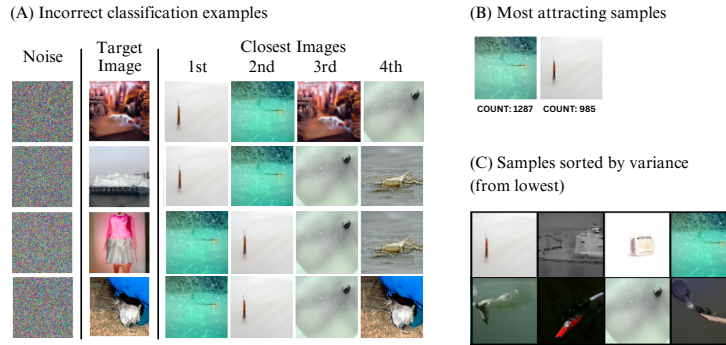


Figure 14: Examples of incorrect assignments of initial noises to resulting images (A), two most noise-attracting images (B), and samples sorted in ascending order by variance of pixels for ADM-64 model trained on the **ImageNet dataset**.

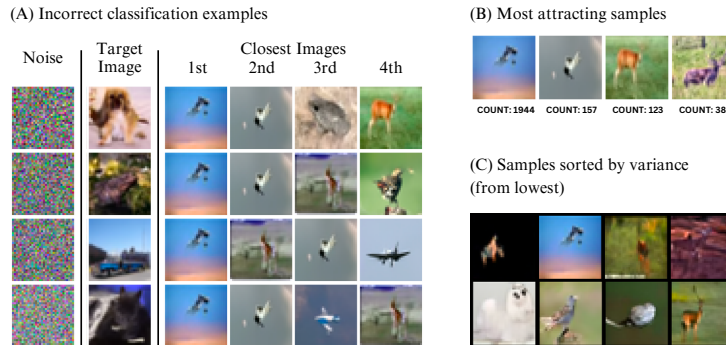


Figure 15: Examples of incorrect assignments of initial noises to resulting images (A), two most noise-attracting images (B), and samples sorted in ascending order by variance of pixels for ADM-32 model trained on the **CIFAR-10 dataset**.

Conclusion. Those findings, connected with the experiment showing reduced diversity of latents (table 4), suggest that the DDIM latents, unlike noise, cannot be accurately assigned to samples, as the approximation error brings them towards the mean, reducing their diversity and making them closest to most of the images.

M On Noise-Image-Latent relations during diffusion training

To further explore the relationships that exist between noises, generations, and latents, we study how the relationships between them change with the training of the diffusion model. We train two diffusion models from scratch and follow the setup from Nichol and Dhariwal [39] for two unconditional ADMs for the ImageNet (64×64) and CIFAR-10 (32×32) datasets. The CIFAR-10 model is trained for 700K steps, while the ImageNet model – for 1.5M steps, both with a batch size of 128. Models employ a cosine scheduler with 4K diffusion steps.

M.1 Spatial relations of noise and latents over training time

We conclude our latent localization experiments (section 3.2) by showing that our observations are persistent across the diffusion model training process. We generate $N = 2048$ images with the final model, using implicit sampling with $T = 100$ steps, and invert them to the corresponding latents using checkpoints saved during the training.

In fig. 16, we show that both the angle adjacent to the noise $\angle x_T$ and the distance between the latent and noise $\|\hat{x}_T - x_T\|_2$ quickly converge to the point that remains unchanged through the rest of the training, indicating that the relation between noises, latents, and samples is defined at the very early stage of the training. Additionally, we observe that the noise reconstruction error in DDIM Inversion does not degrade with the training progress.

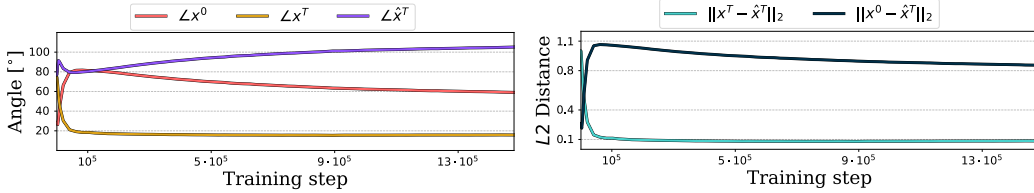


Figure 16: We investigate spatial relations between the noise x_T , latents \hat{x}_T , and generated images x_0 over training process of diffusion model. We show that those relations are defined at the early stage of the training.

M.2 Image-to-noise distance mapping over training time

We analyze the image-noise mapping with l_2 -distance from appendix L over diffusion model training time. We sample $N = 2000$ Gaussian noises and generate images from them using ADM models with $T = 100$ diffusion steps, calculating the accuracy of assigning images to corresponding noises (and vice versa) using the smallest l_2 -distance. In fig. 17, we can observe, for both models, that the distance between noises and their corresponding generations accurately defines the assignment of initial noises given the generated samples ($x_0 \rightarrow x_T$) from the beginning of the training till the end. At the same time, the accurate reverse assignment ($x_T \rightarrow x_0$) can only be observed at the beginning of the training when the trained model is not yet capable of generating properly formed images. Already in the beginning phase of model training, the quality of noise to image mapping rapidly drops and does not change until the end of training.

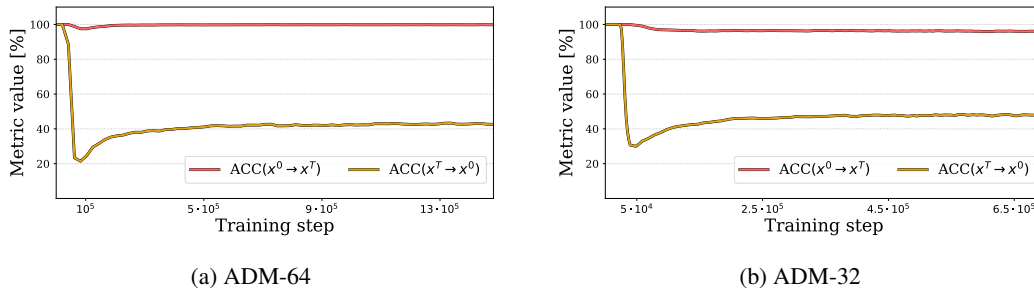


Figure 17: Accuracy of assigning initial noise given the generated sample ($x_0 \rightarrow x_T$) and sample given the initial noise ($x_T \rightarrow x_0$) when training the diffusion model. We can observe that from the very beginning of training, we can assign initial noise with a simple L2 distance while the accuracy of the reverse assignment rapidly drops.

M.3 Image alignment over training time

Inspired by the noise-image mapping experiment, we investigate how the generations resulting from the same noise visually change over DM training time. Thus, for each training step $n \in \{1 \dots 700K\}$ for CIFAR-10 and $\{1 \dots 1.5M\}$ for ImageNet, we generate 2048 samples $\{x_{i,n}^0\}_{i=1}^{2048}$ from the same random noise $x_T^{\text{fixed}} \sim \mathcal{N}(0, \mathcal{I})$, and compare them with generations obtained for the fully trained model. We present the visualization of this comparison in fig. 18 using CKA, DINO, SSIM, and SVCCA as image-alignment metrics. We notice that image features rapidly converge to the level that persists until the end of the training. This means that prolonged learning does not significantly alter how the data is assigned to the Gaussian noise after the early stage of the training. It is especially visible when considering the SVCCA metric, which measures the average correlation of top-10 correlated data features between two sets of samples. We can observe that this quantity is high and stable through training, showing that generating the most important image concepts from a given noise will not be affected by a longer learning process. For visual comparison, we plot the generations sampled from the model trained with different numbers of training steps in fig. 18 (right).

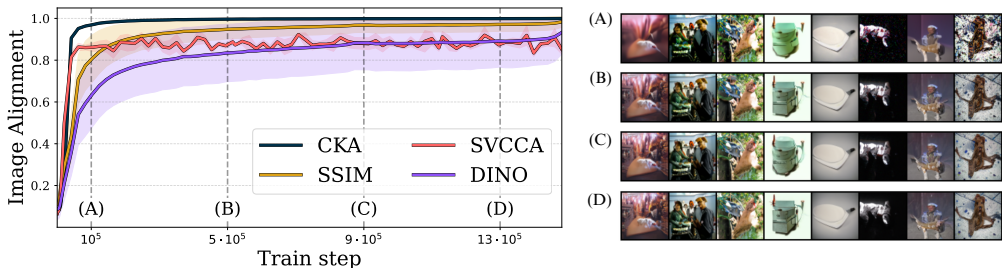


Figure 18: **Similarity of the generations sampled from the same random noise at different stages of diffusion model’s training to the final outputs for ADM-64 model.** Only after a few epochs does the model already learn the mapping between Gaussian noise and generations. Prolonged training improves the quality of samples, adding high-frequency features without changing their content. This can be observed through different image alignment metrics (left) and visual inspection (right).

In fig. 19, we visualize how the diffusion model learns the low-frequency features of the image already at the beginning of the fine-tuning when comparing generations from the next training steps against the generations after finished fine-tuning for the ADM-32 model trained on the CIFAR-10 dataset. In fig. 20 (ADM-64) and fig. 21 (ADM-32), we show additional examples illustrating how generations evolve over training for the same Gaussian noise x_T using a DDIM sampler. Initially, low-frequency features emerge and remain relatively stable, while continued fine-tuning improves generation quality by refining only the high-frequency details.

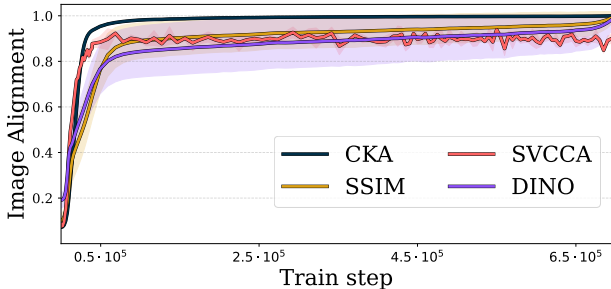


Figure 19: **Similarity of the generations sampled from the same random noise at different stages of diffusion model’s training to the final outputs for ADM-32 (CIFAR-10).** We plot CKA, SVCCA, SSIM, and DINO image alignment metrics and show that the diffusion model already learns the mapping between Gaussian noise and generations at the beginning of the training.



Figure 20: Examples of images sampled using DDIM scheduler from the same noise during the training process for the ADM-64 model trained on the ImageNet dataset.



Figure 21: Examples of images sampled using DDIM scheduler from the same noise during the training process for the ADM-32 model trained on the CIFAR-10 dataset.

N Additional results

In this section, we present qualitative results of replacing first DDIM Inversion steps with forward diffusion.

N.1 Failure cases

As described in section 4, while replacing a higher number of inversion steps with forward diffusion enables better editability of latent encodings (through decorrelating them), it increases the image reconstruction error. In fig. 22, we show that replacing 10% or 20% of first steps can introduce significant changes to images.

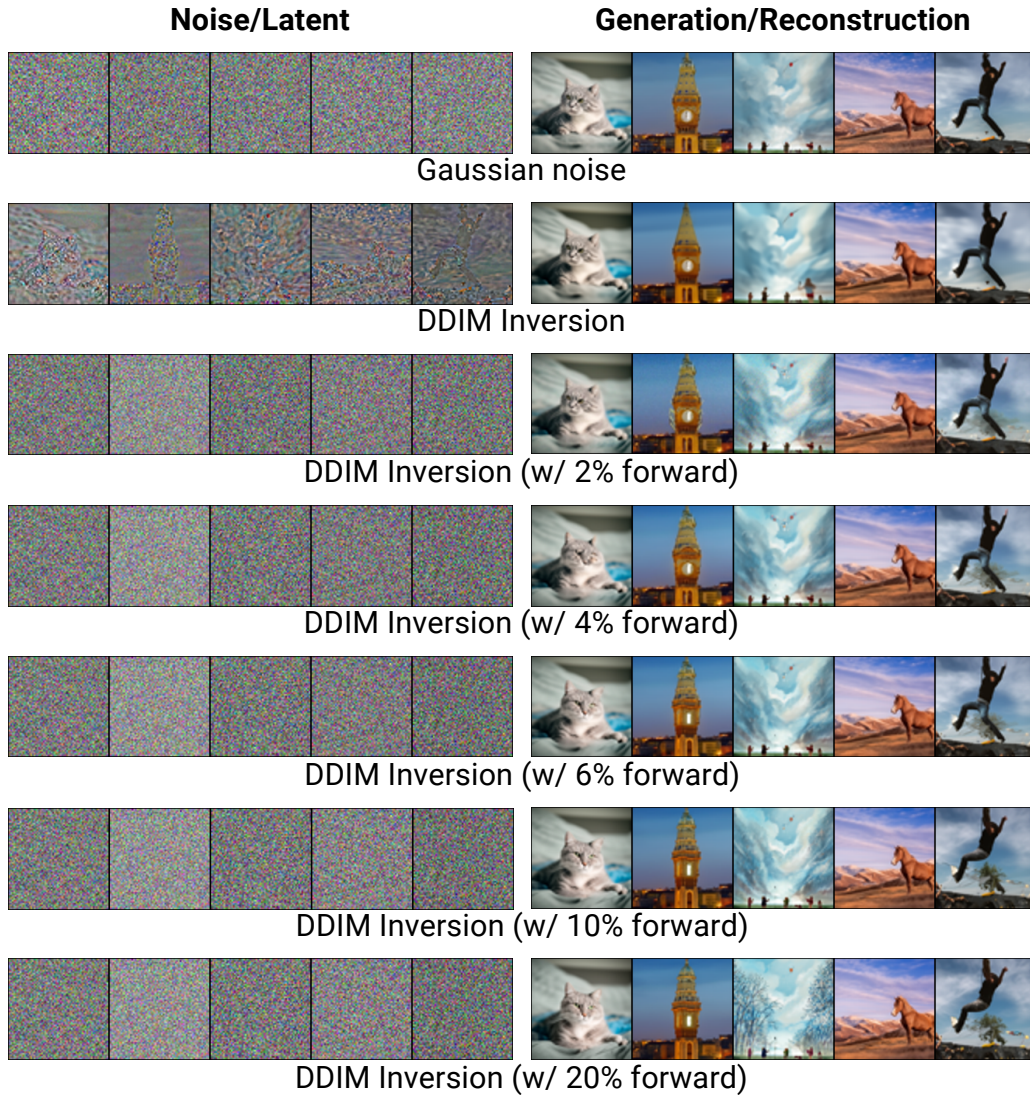


Figure 22: **Replacing first DDIM inversion steps with forward diffusion increases latents editability at cost of a higher reconstruction error.** By replacing from 2% up to 4% of steps we obtain reasonable image reconstructions while removing correlations from latents.

N.2 Interpolation

In section 4, we presented that interpolating DDIM latents with SLERP [48] leads to decrease in image quality and diversity when compared to Gaussian noise. In fig. 23, we qualitatively compare our method for removing correlations in latent encodings with naïve DDIM inversion in the task of image interpolation.

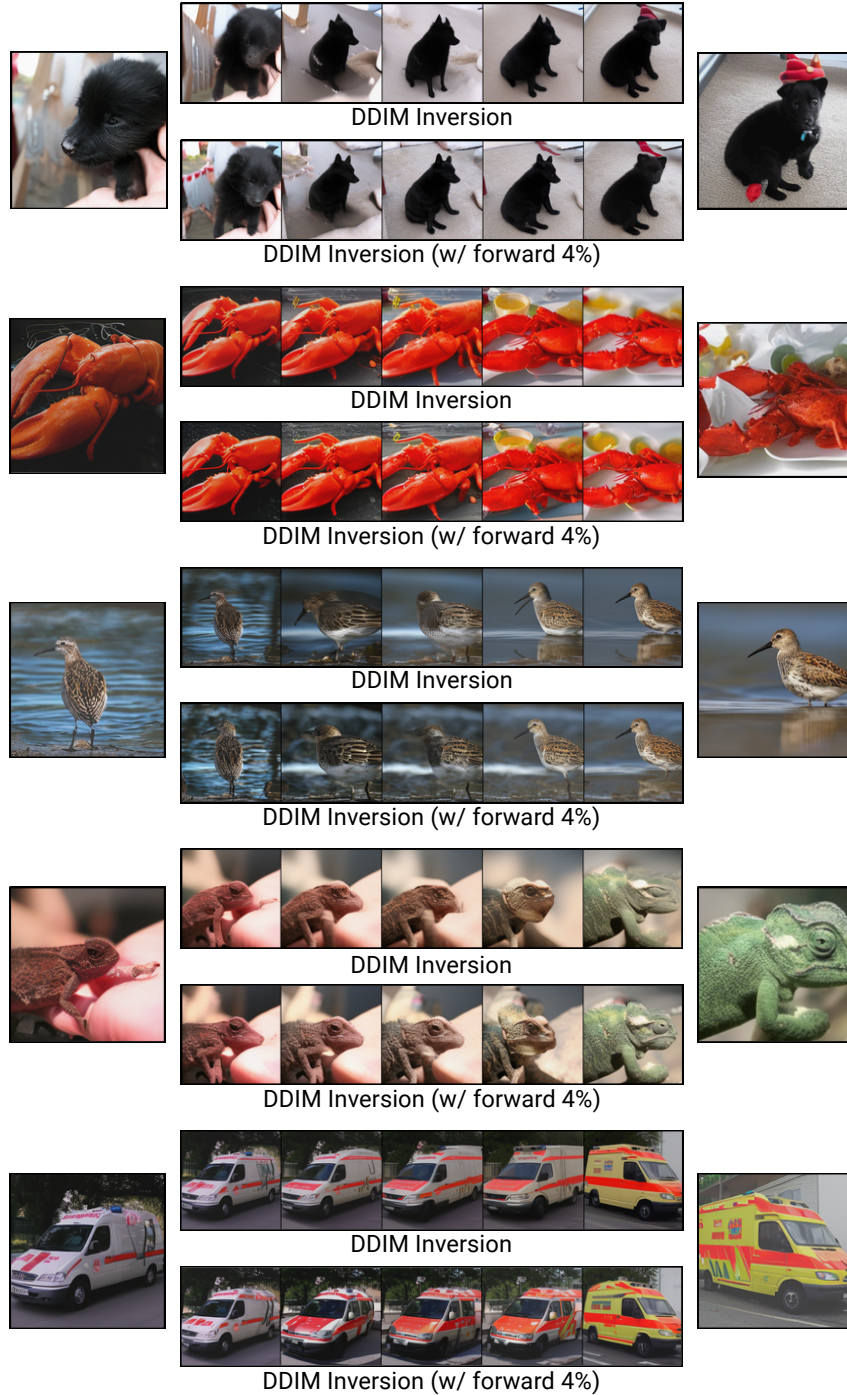


Figure 23: **Qualitative comparison of images generated from interpolated latents produced with DDIM Inversion and our approach.** Contrary to naïve DDIM inversion, proposed solution enables generating high quality objects with pixel-diverse background.